Investigation of fuel and water injection in gas turbine combustion

- Evaluate the methodologies available in Star CCM+ for modeling of water injection in simplified combustor using liquid and gas fuels

Sanger Shinwari

LINKÖPINGS UNIVERSITET

Linköping University | Department of Management and Engineering
Master's thesis, 30 credits| Master's program
Spring 2023| LIU-IEI-TEK-A--23/04682--SE

Linköping University | Department of Management and Engineering
Master's thesis, 30 credits| Master's program
Spring 2023| LIU-IEI-TEK-A--23/04682--SE

Investigation of fuel and water injection in gas turbine combustion

- Evaluate the methodologies available in Star CCM+ for modeling of water injection in simplified combustor using liquid and gas fuels

---

Sanger Shinwari

Academic supervisor: Jörg Schminder
Industrial supervisors: Natalia Korolkova, Daniel Lörstad
Examiner: Hossein Nadali Najafabadi

LINKÖPINGS UNIVERSITET

Linköpings universitet
SE-581 83 Linköping, Sweden
013-28 10 00, www.liu.se

LINKÖPINGS UNIVERSITET

Linköping University | Department of Management and Engineering
Master's thesis, 30 credits| Master's program
Spring 2023| LIU-IEI-TEK-A--23/04682--SE

Abstract

The negative impact of gas turbine emissions on the environment and human health is a growing concern. Recent studies suggest injecting water into the combustion process effectively reduces emissions and increases power output. However, this approach presents new challenges that need to be thoroughly investigated. Siemens Energy (SE) has recently conducted a study on water injection and its effects on gaseous combustion mixtures but encountere challenges the simulation results when adding water. Therefore, the primary objective of this thesis is to evaluate the methodologies available in Star CCM+ for modeling water injection in a simplified combustor model (SCM) using both liquid (diesel) and gas (methane) fuels. In addition, the behavior of the flame, temperature field inside the combustor, and burner outlet temperature, are investigated.

The study has compared physical phenomena such as, the flame shape, velocity, and vorticity field of SCMs with the complete combustor model of the SGT-800 gas turbine for gas fuel. Additionally, the thesis has examined the capability of STAR CCM+ for predicting flame temperature at the outlet against in-house calculation data and Cantera software for parametric cases. The methodology involves a parametric study using the Realizable k-ε Two-Layer turbulence model for steady-state RANS simulations. Combustion is modeled using the FGM method, while Lagrangian multiphase approach is used for liquid injection.

The employed FGM combustion model, Lagrangian multiphase model, and RANS simulations yielded realistic results. In addition, the convergence of gas fuel cases was smoother compared to liquid fuel cases, which involved multiphase modelling and evaporation, makes it more complex. The physical phenomena were captured by CFD simulations for the SCM. Flame shape, velocity and vorticity field have good agreement with the theory in the field of gas turbine combustion and other literature sources. Disagreements between CFD and in-house calculations were observed, with the greatest differences being 24 ℃ for premixed methane (at WFR (Water Fuel Ratio) of 0) and 28 ℃ for non-premixed diesel (at WFR of 1). On the other hand, Cantera results for Vapor and for methane cases with water addition were in limit of 10 ℃ with CFD results for WFR between 0-0.5. Nevertheless, achieving a simulation accuracy within a 10 ℃ limit proved challenging due to limitations and potential sources of error in the in-house calculation sheet, combustion modelling, RANS simulations, and reaction mechanism.

Key words: Diesel and Methane fuel combustion, FGM combustion model, Lagrangian multiphase modelling, Inert Stream, Water injection, STAR CCM+

Acknowledgments

I am delighted to express my gratitude to the individuals and organizations that have contributed to the successful completion of my master's thesis at Siemens Energy in Finspång.

First and foremost, I would like to extend my heartfelt appreciation to Saeid Kharazmi and my industrial supervisor Daniel Lörstad for giving me the invaluable opportunity to conduct my research at Siemens Energy. Their guidance, support, and encouragement have been instrumental in shaping my academic journey, and I am grateful for their trust in my abilities.

I want to sincerely thank my second industrial supervisor Natalia Korolkova, who provided me with invaluable support and assistance in using the CFD software STAR CCM+. I would also like to express my deep appreciation to the combustion operation group at Siemens Energy, particularly Jacek Janczewski, Frank Rubensdörffer, and Prashant Salimath, for their valuable input and support during my research. Finally, I would also like to acknowledge Eduardo Santos Farias at STAR CCM Support Center for his invaluable help and support with CFD simulations.

I am grateful to my academic supervisor and examiner at Linköping University, Jörg Schminder, and Hossein Nadali Nadjafabadi, for their guidance and feedback throughout my research. Their valuable insights and suggestions have significantly contributed to the quality of my work.

Lastly, I want to thank my parents, family members, and friends for their unwavering support, encouragement, and love throughout my academic journey. Their faith in me has been a constant source of motivation and inspiration. I am deeply grateful for their presence in my life.

Thank you all for your invaluable contributions, support, and encouragement.

Sanger Shinwari
Finspång, 2023

Nomenclature

Latin

Symbol	Description	Unit
T	Temperature	K
A	Area	m^2
p	Pressure	Pa
U	Velocity magnitude	$m\ s^{-1}$
y^+	Non-dimensional wall distance	-
Q	Heat flux	Wm^{-2}
D	Droplet diameter	m

Greek

Symbol	Description	Unit
μ	Dynamics viscosity	$kg\ m^{-1}\ s^{-1}$
v	Kinematic viscosity	$m^{-1}s^{-1}$
ρ	Density	kgm^{-3}
σ	Surface tension	Nm

Abbreviations and Acronyms

Letter	Description
CFD	Computational fluid dynamics
CO2	Carbon dioxide
DNS	Direct numerical simulation
LES	Large eddy simulation
FGM	Flamelet generated manifold
LiU	Linköping University
NOx	Nitrogen oxide, toxic emission
STAR-CCM+	Commercial CFD code
We	Weber number
SE	Siemens Energy
SCM	Simplified Combustor Model
CAD	Computer-aided design
WFR	Water Fuel Ratio

Contents

1. Introduction

This chapter is divided into several sections that provide an overview of the thesis. First, it includes a brief background about industrial gas turbines. Then, it reviews previous studies on the topic and describes the problem this thesis aims to address. Next, the chapter presents the objectives of the thesis, along with any prerequisites and restrictions that need to be considered. Finally, an outline is presented that gives a general overview of the structure of the thesis.

1.1 Background

Industrial Gas Turbines are essentially turboshaft engines that convert the chemical energy of fuel into mechanical energy through a continuous combustion process. The gas turbine consists of three essential components: an air compressor, a combustion chamber (burner), and a turbine as shown in Figure 1 (1). The compressor compresses the air and forces it into the combustion chamber, where it is mixed with fuel and ignited, increasing the thermal energy of the air/fuel mixture. Finally, the hot gas from the combustion expands through the turbine, rotating the blades and generating mechanical energy. This energy from the gas turbine is utilized in various industries such as oil, land transport (trains), cargo ships, hydrofoils, and power plants. Modern gas turbines are fuel-flexible and can run on different fuels, such as natural gas, diesel fuel, crude, vaporized fuel oils, naphtha, and biomass. Each fuel has advantages and challenges, depending on the energy density, environmental impact, availability, compatibility, and cost (1). Methane, also known as natural gas (CH_4), is a popular fuel source used in gas turbines as fuel. Methane has a better carbon intensity than diesel fuel due to its higher hydrogen-carbon ratio and is more flammable than diesel. However, it has a much lower fuel density. It means more methane is needed to produce the same energy as fossil fuel (diesel) (2). Diesel fuel is more viscous and has different spray characteristics that can impact combustion. The fuel choice depends on the application, efficiency, emissions, and flame stability.

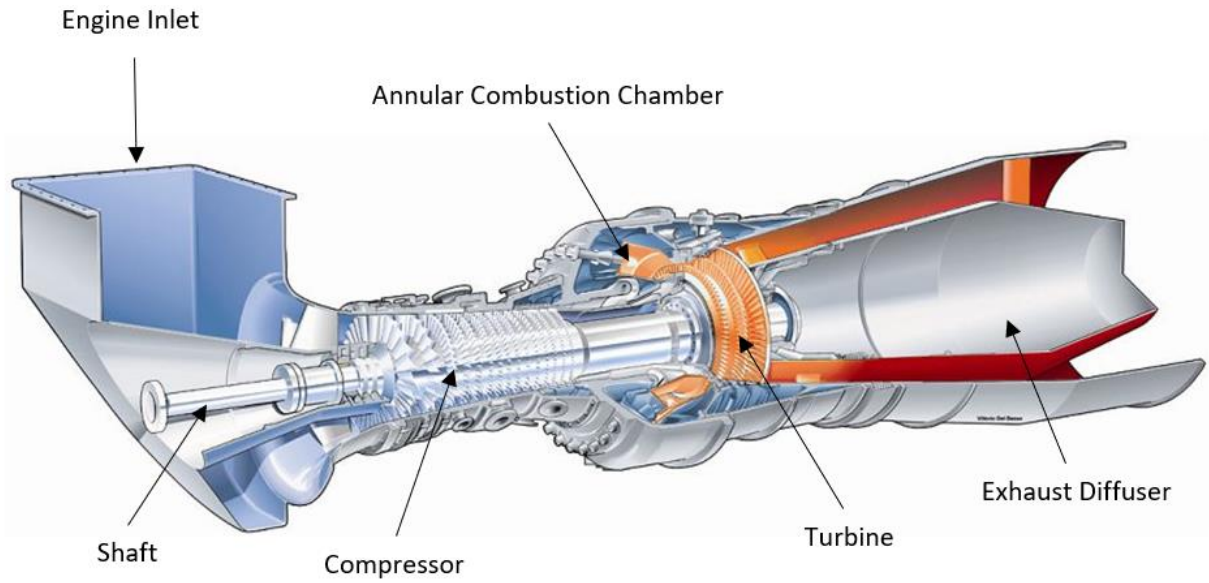

Figure 1: General layout of SGT-800 industrial gas turbine

The combustion process of gas turbines emits several pollutants, including carbon dioxide (CO_2), nitrogen oxides (NOx), and unburned hydrocarbons (UHC). It is well-known that CO_2 contributes to climate change, and NOx emissions lead to smog and acid rain forming,

negatively impacting human health and the environment (1). Therefore, it is essential to use high-quality fuels with low-emission rates, advanced combustion technologies, and emissions control equipment to reduce these emissions.

Therefore, water injection has recently gained significant attention as a potential solution for reducing emissions from gas turbine combustion. The injection of water into the combustion process can lower the production of pollutants such as NOx while increasing the efficiency of the gas turbine (3)- (4). However, the addition of water during the combustion process presents new challenges. Therefore, it is crucial to understand the behavior of the combustion process with water injection and investigate various parameters such as flame behavior, temperature field inside the combustor, outlet temperature from the burner, and other factors to determine the effectiveness of water injection in reducing emissions.

In conclusion, it is crucial to study the behavior of different fuels together with water injection inside the combustion chamber of a gas turbine. Testing a new fuel mixture brings challenges, so it is essential to study the behavior of the flow and combustion inside the chamber. A deeper understanding of the combustion process for different fuels with water injection will highlight areas for improvement in efficiency, low emissions, and stable combustion. Investigating this by experiments is difficult and expensive, but with Computational Fluid Dynamics (CFD) simulations, it can be studied using numerical methods and algorithms. CFD simulations have emerged as a crucial tool for evaluating and analyzing combustion processes across a range of applications. They offer an economical alternative to constructing and altering prototypes. The calculations are performed by establishing fundamental conservation equations and solving them through numerical methods. Nonetheless, resolving most combustion problems requires substantial computer capacity due to the turbulence and complexity of the flow. Numerous commercial CFD codes are now accessible for conducting simulations, each with specific constraints. It is vital to recognize these limitations before drawing any conclusions.

1.2 Literature Study

Computational fluid dynamics has become a popular tool in recent years for simulating the combustion chamber of gas turbines for various purposes. However, adding water injection into the combustion chamber is a novel idea in the industry, making it difficult to find related studies for this thesis work. Therefore, the literature study for this thesis aims to assess CFD's ability to simulate combustion processes and multiphase flow in similar problems. The literature study covers various topics, such as multiphase flow simulations, spray modeling, flame stability, emissions from combustion, gas turbine combustion performance, injection of liquid fuel/water vapor, flow swirl, non-premixed combustion, and other related topics.

G. Bulat et al. conducted a simulation of an industrial gas turbine combustor (Siemens SGT-100) using Large Eddy Simulations (LES) and the sub-grid probability density function (PDF) method (5). The sub-grid PDF method uses a set of equations to track changes in the sub-grid scale PDFs, taking into account both the impact of the resolved large-scale flow on sub-grid scale fluctuations and the effect of sub-grid scale fluctuations on the resolved large-scale flow. In the simulation, natural gas (96.97% CH_4) with a temperature of 319.8 K was injected through multiple holes in the swirl vanes. The results showed good agreement with experimental data in the flame area at various axial positions, and the method also accurately reproduced the measured levels of NO emissions. In conclusion, the results indicate that it is possible to simulate complicated combustion issues in industrial geometries using LES with a sub-grid PDF model with simplified chemical reactions.

S. A. Inam et al. simulated the supercritical combustion of gaseous hydrogen and liquid oxygen through CFD (6). Pressure-based steady-state simulation using different turbulence models such as standard k–ε, standard k–ω, and SST k–ω models with ideal and real gas assumptions were carried out for non-premixed combustion. The simulation results showed that the SST k–

ω turbulence model with real gas assumption is not only qualitatively accurate but also quantitatively consistent with the experimental data. The authors suggest that the results will significantly improve by using more advanced modelling techniques and incorporating a more comprehensive chemical kinetic mechanism.

X. Chen et al. studied the combustion performance of a biogas micro gas turbine through 3D numerical analysis (7). The RNG k-ε turbulent model, an eddy-dissipation/finite rate model, and an eight-step chemical reaction mechanism were used during this simulation. The most significant error is around 10% between numerical data and experimental for validation variables such as fuel rate, average temperature, and NO concentration (at 15% oxygen) at the outlet. The results showed that as the proportion of CO2 in the fuel increases, the temperature of the combustor head decreases slightly, along with a reduction in the emission concentrations of NO and CO.

T. D. Naguen et al. examines the flow dynamics within the gas turbine engine (GTE) combustion chamber's swirled, focusing on the impact of varying blade angles on the mixing ratio (8). Results from experiments were compared to those obtained through numerical simulations, utilizing various models of turbulent viscosity such as stationary RANS equations of k–ε and k–ω families; nonstationary model of LES; and combined DES (Detached-Eddy Simulation) and SAS (Scale-Adaptive Simulation). The results showed that the k-ε RNG model from the RANS models of the k–ε and k–ω families show the best performance. Additionally, when it comes to transient calculations, the DES model provides the closest results to experimental data.

M. B. Gil studied the flow field and liquid spray injection in a Lean Direct Injection (LDI) gas turbine combustor using Eulerian-Lagrangian LES and U-RANS (9). Like traditional fuel injection systems, an LDI system injects fuel directly into the combustion chamber instead of the intake manifold. LDI aims to burn fuel more thoroughly, increasing fuel efficiency and reducing emissions. U-RANS and LES simulations were found to align with the experimental data regarding the predicted location and size of the recirculation zones and the average and fluctuating air velocity components. The LES simulations also showed a flow pattern matching the highly swirled configurations in the experiments.

M. Persson investigated the diesel fuel system inside the SGT 750 combustion chamber developed by Siemens Industrial Turbomachinery using CFD software STAR CCM+ (10). Steady-state simulations were conducted using the SST k-ω turbulence model, and the liquid fuel option was modelled as a multiphase problem using a Lagrangian framework. Furthermore, combustion was modelled using Flamelet Generated Manifold (FGM) table. As a conclusion of his thesis, the larger angle of the injector gives better mixing but increases the maximum residence time. Among other things, M. Persson also investigated diesel and methane gas which showed that gas has more even equivalence ratio distribution than diesel as fuel.

R. Agbadede et al. investigated the effect of water injection into an aero-derivative gas turbine combustor on NOx reduction (3). A twin-shaft aero-derivative gas turbine simulation was created and run using the GASTURB simulation software. Then, a simulation was conducted to examine the effect of adding water to the gas turbine combustor, with water-to-fuel ratios ranging from 0 to 0.8, increasing by 0.2 each time. The results indicate that the NOx severity index decreased as the water-to-fuel ratio increased. On the other hand, the heat rate and fuel flow also increased.

V. A. Kuznetsov numerically studied the effects of superheated steam supply during the combustion of liquid fuel in a burner (11). N-heptane was used as the model fuel, and the flow of gases was modeled with the RANS approach. In addition, the Eddy dissipation concept (EDC) was used to simulate combustion, reducing the chemical reaction mechanism. The

calculations' results aligned with the experimental data, specifically regarding the key integral parameters. Additionally, the study demonstrated that injecting steam into the combustion zone effectively reduces emissions of nitrogen oxides and carbon monoxide.

R. Sharafoddin et al. studied the effect of water vapor injection on the flow pattern, temperature contamination, and emission of pollutants in the combustion chamber of a gas turbine (4). The effect of the angle at which the spray hits the axis has been examined, as well as the influence of fuel type and the object's shape on the flow characteristics. The second-order Euler method is used for the discretization of governing equations, and the standard k-ε turbulent model is used for modelling turbulence. The study found that when a certain amount of water was added, the temperature and pressure in the combustion chamber changed significantly. Additionally, it was discovered that injecting 8% water into the Brighton cycle improved the overall efficiency from 91% to 95%.

D. Lörstad et al. investigated both LES and RANS simulations to analyze the behavior of the SGT-800 gas turbine burner, explicitly focusing on the transient fuel distribution and flame behavior (12). The LES calculations employed a combustion code developed from the OpenFOAM library, incorporating a mixed subgrid flow and subgrid wall models. In addition, a Finite Rate Chemistry (FRC) combustion model based on the Partially Stirred Reactor (PaSR) model was also used to simulate the reacting flow. On the other hand, the RANS simulations were performed using ANSYS Fluent, employing the k-ε Realizable eddy viscosity turbulence model in conjunction with the Fluent partially premixed combustion model. Results showed that the LES calculations were able to predict the flame position more accurately than the corresponding RANS simulations, and the flame shape appeared reasonable. However, there is room for improvement in the LES RMS fluctuation levels, which were underpredicted compared to the high measurement levels. Finer grids, advanced kinetic schemes, or updated boundary conditions may be necessary to address this.

Based on the literature review, it is evident that CFD is a valuable tool for examining gas turbine combustion with its limitation. Moreover, the impact of water injection has also been acknowledged in some studies, and it has been demonstrated that water injection can decrease emissions from the gas turbine combustion process. Different methods were observed for modeling combustion and choosing turbulent models. In CFD, the model selection depends on the industrial model's complexity and the parameters that need to be studied. As a result, different approaches were taken in the above studies to address specific problems.

1.3 Problem Description

Gas turbines release a range of pollutants that negatively impact the environment and human health, with CO2 being a major contributor to climate change and NOx emissions leading to smog and acid rain (1). Based on recent studies by R. Agbadede et al. (3), V. A. Kuznetsov (11), and R. Sharafoddin et al. (4) suggest that the injection of water into the combustion chamber can reduce emissions from gas turbine combustion due to reduction in peak flame temperature which reduces the formation of NOx. Furthermore, water addition can boost power as well due to increase in the mass flow rate. However, the addition of water during the combustion process presents new challenges. Therefore, it is essential to investigate various parameters, such as the behavior of the flame, temperature field inside the combustor, burner outlet temperature, and other factors, to determine the effectiveness of water injection in reducing emissions. By understanding the behavior of the combustion process with water injection, researchers can optimize the process to mitigate the negative impact of gas turbine combustion on the environment and human health.

Siemens Energy (SE) has recently studied water injection and its effects on gaseous combustion mixtures to reduce NOx emissions and boost power. CFD was used to predict the temperature profile at the combustor outlet for methane as gas fuel and water injection case.

However, SE detected question marks of the Star CCM+ accuracy of calculating the flame temperature when adding water, the simulation results did not align well with the experimental data. To address this issue, SE suggested developing a methodology for water injection into the combustion process using CFD code STAR CCM+. The capability of STAR CCM+ for predicting the flame temperature at the outlet of the combustor will be examined by performing a parametric study. The parametric study consists of several cases for liquid (Diesel) and gas (Methane) fuel and water injection. Moreover, it is also suggested to use a simplified combustor model (SCM), which will save computational time and easy to mitigate challenges.

1.4 Objective

The primary objective of the thesis is to evaluate the methodologies available in Star CCM+ for modeling of water injection in SCM using liquid (diesel) and gas (methane) fuels. The characteristic of the SCM's regarding the flame shape and vorticity field will be compared with the complete combustor model of the SGT-800 gas turbine for gas fuel. Additionally, the goal is to gain a deeper understanding of the combustion process and how different fuel types, together with water injection, affect the flame temperature at the combustor outlet. Finally, the capability of STAR CCM+ will be validated for predicting flame temperature at the outlet against in-house calculation data for the parametric cases. The difference of 10 ℃ between CFD and in-house calculations is considered good enough. In addition to these primary objectives, the following questions will also be investigated during this master's thesis:

- What are the modeling requirements to simulate water injection for the SCM regarding geometry simplification, multiphase and combustion modeling?
- How the physical phenomena such as flame shape, velocity, and vorticity have been captured using the employed method in relation to theory and available literature sources?
- How does the flame temperature at the outlet varies for parametric cases and how these findings correlate with in-house calculations?

1.5 Delimitation

This thesis is limited to 30 academic credits, equivalent to 800 hours of work. The study is expected to be completed by the end of May 2023, within a 20-week timeframe. The methodology will be only based on what is currently available at CFD software STAR-CCM+, including the pre-processing, simulation, and post-processing phases.

No experiments will be carried out as part of this thesis. The study will be purely numerical and based on CFD simulation, with in-house calculation data provided by SE. Adequate computational resources will be available for conducting the numerical simulations. Only steady-state RANS simulation will be performed in this project for all the cases. Furthermore, the author is partly dependent on the help of others when deciding the boundary condition of the combustion chamber and geometry simplifications. The dependence on other persons requires good planning, and the control is not only in the author's hands.

1.6 Report Outline

The opening chapter of the thesis thoroughly outlines the theories required for understanding the research. The study then delves into the fundamentals of fluid dynamics and CFD, starting

with a general theory on gas turbine combustion systems. Lastly, theories specific to the study are presented to enhance knowledge and understanding.

In chapter three, the methodology is outlined with a focus on the modeling process, including creating models from available information. The most noteworthy results are presented and discussed in later chapters, highlighting the study's major findings. The conclusion then ties the findings to the theories presented, offering suggestions for further research and prospects.

2. Theoretical background

In this chapter, the required theory for understanding this work is presented. A brief overview of industrial gas turbine combustion system, the basics of CFD, and the various models and methods utilized in this project are provided. For further details, the reader is referred to additional sources.

2.1 SGT-800 Gas Turbine Combustion System

The SGT-800 gas turbine in Figure 1 is a 50 MW single-shaft gas turbine equipped with a 3rd generation Dray Low Emission (DLE) combustion system (14). SGT-800 consists of 30 burners with an annular-shaped combustion chamber (15). The burner is located upstream of the combustion chamber and is a critical part of the gas turbine responsible for mixing the fuel with the compressed air from the compressor.

To facilitate this mixing process, the gaseous fuel enters the burner through the main gas pipes positioned on a swirl cone, as shown in Figure 2. The cone features slots that serve as a swirl generator, initiating the mixing of the gas and air. Next, the gas is injected through holes in the main gas pipes, and the mixing process continues in the mixing tube. Finally, fuel and air are combined in the mixing tube to form a homogeneous mixture ready for ignition. When the mixture reaches the burner outlet and enters the combustion chamber, it is ignited, and the combustion process begins (15).

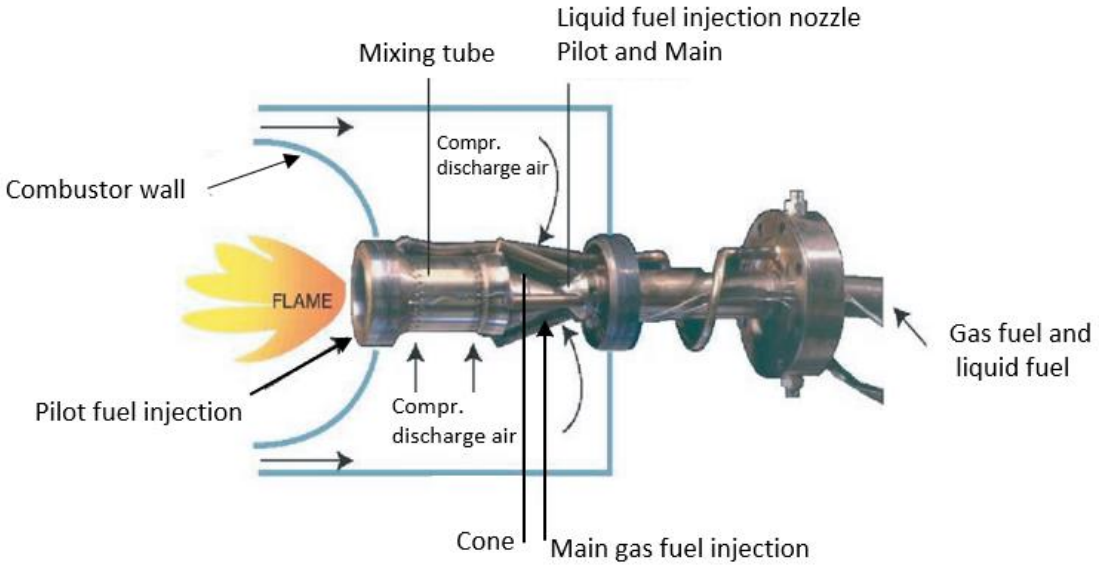

Figure 2: DLE burner system configuration, figure taken from (13)

The air distribution in the DLE burner is illustrated in Figure 3 , where it is shown that the majority of the airflow (85%) enters through the cone slots of the burner. Additionally, 10% of the air enters the mixing tube via four rows of tiny film holes. The center of the burner receives a minor proportion of the remaining airflow (3%), while the pilot flame combustion process involves the remaining 2% (16). Furthermore, the burner has four injection points for fuel. In Figure 3, these injection points are located on the space cap, which has four holes labeled as A, B, C, and D. In addition, gaseous fuel is also injected through holes in the swirl cone cylinders, labeled as 0-8 in Figure 3 (17).

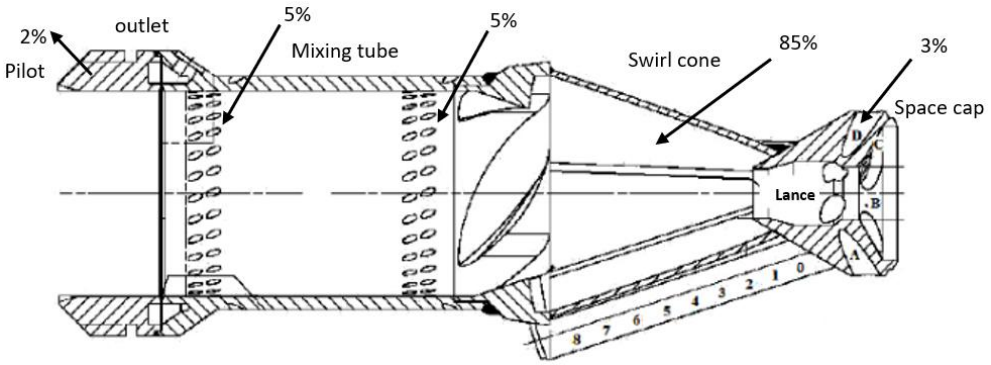

Figure 3: Air distribution in DLE burner, figure taken from (14).

The swirl cone equipped with twisted vanes creates flow rotation and gives a swirl velocity profile that improves the mixing of air and fuel. This mixture moves through the mixing tube and reaches the burner outlet. Furthermore, the center of the mixing tube has the highest velocity, which hinders the pre-ignition of the gas-air mixture within the tube. The film holes in the mixing tube help prevent gas ignition along the walls (15). The pilot holes, used for injecting gaseous and liquid fuel, are located on the outer ring of the burner outlet and are used for stabilizing the combustion process. Additionally, liquid fuel can be injected through the lance at the center of the space cap shown in Figure 3.

The flow pattern inside the mixing tube and at the outlet is shown in Figure 4. As the fuel-air mixture enters the combustion chamber, it is expanded in a radial direction and mixed with combustion due to the swirling action. A phenomenon known as vortex breakdown occurs close to the burner outlet, where the swirl flow is expanded into the combustion chamber (16). This vortex breakdown creates a large vortex structure and a central recirculation area where combustion products recirculate. This recirculation zone and vortex breakdown are crucial in local flame stabilization (17). The recirculation zone of flow in combustion systems allows for the longer residence time of combustion products in the combustion chamber, permitting sufficient time for combustion reactions—this prolonged residence time results in complete fuel combustion and improved combustion efficiency. The high-temperature products generated during the combustion reactions also serve as a stable ignition source for the flame, ensuring continuous and stable combustion (18).

If the swirl's axial velocity is too low, the stagnation point and the flame may move back into the mixing tube, leading to a flashback. In other words, a flashback occurs typically when the flame moves towards the fresh gases upstream at a velocity greater than the inflow velocity (19). Conversely, if the axial velocity is too high, the flame will be pushed out into the combustion chamber and become unstable. The pilot flame is designed to support the primary flame, and the optimal location is to enter between the recirculation zones and the primary flame zone (13).

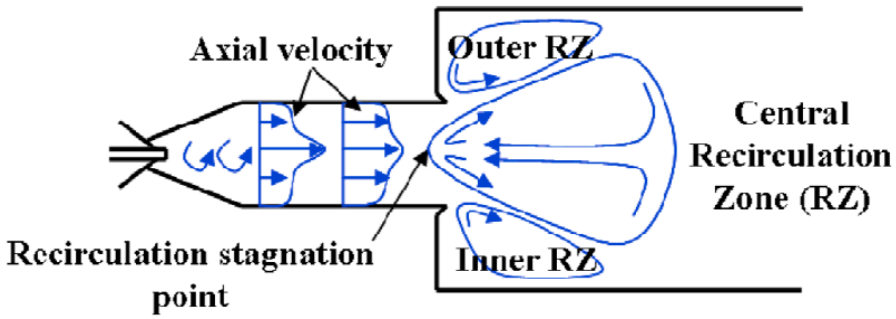

Figure 4: Flow pattern inside mixing tube and at burner outlet, figure taken from (14).

Moreover, liquid fuel combustion involves mixing the spray of droplets with air, transforming the droplets into vapor, decomposition of heavy hydrocarbons into lighter components, thoroughly mixing these hydrocarbon molecules with oxygen, and finally, the chemical reactions that take place. For combustion to occur effectively and quickly in a moving air stream within a limited space inside the combustor, it is crucial to have a high temperature, which can be achieved by burning an approximately balanced mixture (stoichiometric mixture). A stoichiometric mixture is a mixture of fuel and oxidizer that is balanced to avoid excess of either component after combustion. This will ensure that all the processes involved occur at a fast enough pace. In reality, the air-to-fuel ratio used for combustion is much leaner than the stoichiometric ratio. This is done to reduce the turbine's inlet temperatures, as practical limitations need to be considered (20).

2.2 Computational Fluid Dynamics

Computational Fluid Dynamics uses computer simulations to analyze systems involving fluid flow, heat transfer, and related processes like chemical reactions. It is a powerful technique with many applications in both industrial and non-industrial fields. Since the 1960s, the aerospace industry has incorporated CFD techniques into designing, developing, and producing aircraft and jet engines. CFD software is built around numerical algorithms that can handle fluid flow issues. To make it easy for users to utilize its capabilities, all commercially available CFD packages include advanced user interfaces for entering problem parameters and viewing results (21).

Fluid dynamics studies fluids' movement, behavior, and characteristics, such as liquids and gases. It is based on three governing principles that help explain and predict the actions of fluids in various conditions. These principles are the conservation of mass, the conservation of momentum, and the conservation of energy.

Governing principle of conservation of mass states that the rate of mass increase in the fluid element is equal to the net rate of mass flow into the fluid element. This principle can be written in mathematical form presented in equation (1), called the continuity equation. Equation (1) is written in unsteady and three-dimensional mass conservation form where ρ is the density and $\mathbf{v}$ is the velocity vector.

$$\frac{\partial \rho}{\partial t} + \nabla \cdot (p\mathbf{v}) = 0 \tag{1}$$

Conservation of momentum is based on Newton's second law which states that the rate of change of momentum of a fluid particle equals the sum of the forces on the fluid particle. Momentum is a quantity with both magnitude and direction; therefore, its conservation must hold in all directions. This is represented by equation (2) where $\otimes$ is the Kronecker product, p the pressure, $\mathbf{T}$ the viscous stress tensor, and $\mathbf{f}_b$ is the resultant body forces.

$$\frac{\partial (\rho \mathbf{v})}{\partial t} + \nabla \cdot (\rho \mathbf{v} \otimes \mathrm{v}) = -\nabla \cdot p\mathbf{I} + \nabla \cdot \mathbf{T} + \mathbf{f}_b \tag{2}$$

Lastly, the first law of thermodynamics serves as the foundation for the conservation of energy equation, which states that a fluid particle's energy change is the result of the heat added to the fluid and the work performed on the particle. This is represented by equation (3), where E is the total energy per unit mass, S_E is the energy source per unit volume, and $\mathbf{q}$ is heat flux.

$$\frac{\partial (\rho E)}{\partial t} + \nabla \cdot (\rho E \mathbf{v}) = \mathbf{f}_b \cdot \mathbf{v} - \nabla \cdot \big(\mathbf{v}(p\mathbf{I} + \mathbf{T})\big) - \nabla \cdot \mathbf{q} + S_E \tag{3}$$

The motion of the fluid is described by five partial differential equations, mass conservation, momentum equations in x-, y- and z-directions, and energy equations as mentioned above. The governing equation is solved numerically by implementing it into a control volume, and it is discretized with respect to time and space. However, to solve governing equations numerically the equation of state should be taken into consideration. The most common equation of state is the ideal gas law.

In the flow of compressible fluids, the equations of state connect the energy equation with the mass conservation and momentum equations. This connection is a result of changes in density due to variations in pressure and temperature in the flow field. However, liquids and gases flowing at low speeds act as incompressible fluids, where the energy equation does not need to be considered. The flow field can be solved using only the mass conservation and momentum equations unless heat transfer is involved, in which case the energy equation must also be considered.

Moreover, the Reynolds number, represented by equation (4) in fluid mechanics, is crucial in determining the nature of fluid flows. It is computed as the ratio of inertial forces to viscous forces. It depends on various factors such as velocity (u), a characteristic length (l), density (ρ), and dynamic viscosity (μ).

$$Re = \frac{\rho u l}{\mu} \tag{4}$$

The Reynolds number categorizes fluid flows into three states: laminar, turbulent, or transitional. In laminar flow, fluid particles move smoothly in layers, whereas in turbulent flow, they are highly disordered and experience irregular fluctuations and mixing (swirls). For a deep understanding of CFD and fluid mechanics, see (21) and (22).

2.3 Near-wall Treatment

Most practical flow problems involve walls that cause vorticity, making it crucial to accurately predict the flow in the wall boundary layer. The wall boundary layer is the thin layer affected by viscosity near a wall, where the flow velocity transitions from zero to the free stream velocity (U). The nominal thickness of the boundary layer $\delta(x)$ is defined as the normal distance from the wall to a point where the velocity is 99% of U. Viscous stresses can be ignored beyond this point. Depending on the Reynolds number, the boundary layer flow can be laminar or turbulent. The boundary layer is laminar at low Reynolds numbers, and the streamwise velocity changes uniformly away from the wall. At high Reynolds numbers, the boundary layer is turbulent, and unsteady swirling flows within the boundary layer characterize the streamwise velocity. Figure 5 illustrates how the uniform velocity profile transforms into a turbulent boundary layer as the flow continues along the wall. The turbulent boundary layer consists of two layers: the outer layer, dominated by turbulence, and the inner layer, with three sublayers. In contact with the wall, the viscous sublayer is mainly laminar and affected by viscosity. The log layer is equally influenced by turbulence and viscosity, and the buffer layer is a transitional zone between the viscous sublayer and the log layer. In the viscous sublayer, the mean velocity depends on fluid density, viscosity, distance from the wall, and wall shear stress.

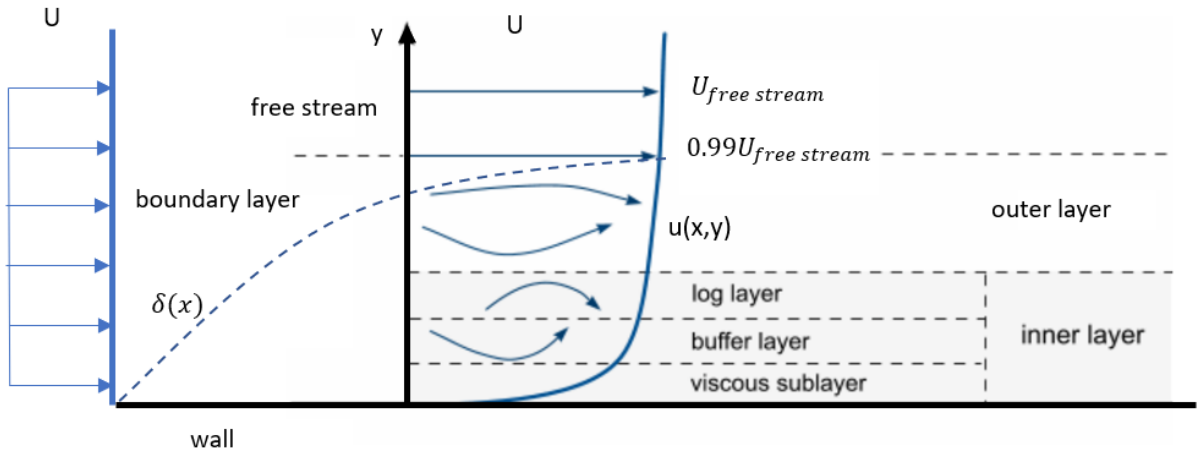

Figure 5: Boundary layer development along a plate.

This implies that predicting the transition region from laminar to turbulent flow is much more complicated than predicting free stream flow. One can determine the position of mesh nodes within the boundary layer by defining a y+ value based on flow characteristics and mesh sizes using equation (5). When the y^+ value is below one, it indicates that the first node is in the laminar layer (viscous sublayer). Conversely, y^+ value above 30 denotes that the node is within the turbulent layer (outer layer). The transitional area between these values represents the flow in transition.

$$y^+ = \frac{u*y}{\nu} \tag{5}$$

2.4 Modelling Turbulence

In engineering problems, flows can be simple, such as two-dimensional jets, pipe flows, flat plate boundary layers, or more complex three-dimensional ones. However, these flows become unstable when the Reynolds number exceeds a certain threshold. At low Reynolds numbers, the flow is smooth and orderly. However, as the Reynolds number increases, the flow becomes turbulent and chaotic, with random and continuous changes in velocity and pressure throughout large flow regions. As a result, many flows in engineering applications are turbulent. Given the significance of avoiding or inducing turbulence in engineering, it's not surprising that a considerable amount of research is devoted to creating numerical methods to accurately capture turbulence's impact. These methods can be classified into three categories, Direct Numerical Simulation (DNS, Large Eddy Simulation (LES), and Reynolds-averaged Navier-Stokes (RANS) method (21).

In DNS simulations, both the average flow and turbulent velocity fluctuations are computed. These simulations solve the unsteady Navier-Stokes equations using a grid system that is finely spaced enough to capture energy dissipation at the Kolmogorov length scales and with small enough time steps to resolve the quickest fluctuations. However, these calculations require a large number of computing resources and, therefore, are not used for industrial flow computations.

LES is an intermediate turbulence calculation method that focuses on the behavior of the larger eddies. The process starts with filtering the unsteady Navier–Stokes equations only to include the larger eddies and exclude the smaller ones. The impact of the smallest unresolved eddies on the resolved flow, which includes the mean flow and large eddies, is then considered through a sub-grid scale model. Although this technique also requires a lot of computing resources, it is increasingly being used to solve complex CFD problems with its unsteady flow equation solution.

Finally, the RANS method is the most cost-effective in CFD, which concentrates on the mean flow and the impact of turbulence on the mean flow characteristics. Before applying numerical techniques, the Navier-Stokes equations are averaged over time (or ensemble-averaged in case of time-varying boundary conditions). The averaged flow equations contain additional terms due to the interaction between turbulent fluctuations, which are modeled using eddy viscosity models. A turbulent entity can be written as equation (6), where $\overline{\emptyset}$ is the mean component and $\emptyset\acute{(t)}$ is the fluctuating component with time t. $\emptyset$ can be velocity components, pressure, energy, or species concentration.

$$\emptyset(t) = \overline{\emptyset} + \emptyset\acute{(t)} \tag{6}$$

The value obtained from equation (5) is then incorporated into the three governing equations and time-averaged to obtain a steady-state solution. The averaged conservation of mass and momentum can be seen in equations (7) and (8), respectively.

$$\frac{\partial \rho}{\partial \mathrm{t}} + \nabla \cdot (\overline{\rho \mathrm{v}}) = 0 \tag{7}$$

$$\frac{\partial}{\partial \mathrm{t}}(\overline{\rho \mathrm{v}}) + \nabla \cdot (\overline{\rho \mathrm{v}} \otimes \overline{\mathrm{v}}) = \nabla \cdot \bar{\mathrm{p}}\mathbf{I} + \nabla \cdot (\mathbf{T} + \mathbf{T}_t) + \mathbf{f}_b \tag{8}$$

The fluctuating component $\emptyset\acute{(t)}$ is presented in equation (8) as a part of Reynold stress tensor $\mathbf{T}_t$; see equation (9).

$$\mathbf{T}_t = -\overline{\rho} \begin{bmatrix} \overline{\acute{u}\acute{u}} & \overline{\acute{u}\acute{v}} & \overline{\acute{u}\acute{w}} \\ \overline{\acute{u}\acute{v}} & \overline{\acute{v}\acute{v}} & \overline{\acute{v}\acute{w}} \\ \overline{\acute{u}\acute{w}} & \overline{\acute{v}\acute{w}} & \overline{\acute{w}\acute{w}} \end{bmatrix} \tag{9}$$

This raises concerns about the closure problem, with more unknown variables than equations. However, this problem is a fundamental aspect of fluid dynamics and turbulence, and a complete and accurate definition has yet to be established (21).

2.5 Eddy Viscosity Models

To predict the movement of fluid in turbulence, the flow characteristics are broken down into average and fluctuating parts through the process of Reynolds decomposition. The Navier-Stokes equations are then reworked with the new quantities to give the RANS. However, the fluctuating components in these equations are unknown, leading to an incomplete system of equations. To resolve this, additional equations known as turbulence models are developed to solve for these missing terms. The most common one is the eddy viscosity models (23).

The eddy viscosity Models, the most widely used models, are based on the Boussinesq assumption proposed by Joseph Valentin Boussinesq. This assumption states that the Reynolds stress is proportional to the average strain (24). This assumption enables the models to study a wide range of flow phenomena. Equation (10) describes this Boussinesq assumption between turbulent viscosity μ_t , and mean strain rate tensor $\mathbf{S}$. k is the turbulent kinetic energy defined as $k = \frac{1}{2}(\overline{u^2} + \overline{v^2} + \overline{w^2})$.

$$\mathbf{T}_t = 2\mu_t \mathbf{S} - \frac{2}{3} k\mathbf{I} \tag{10}$$

The eddy viscosity models solve additional transport equations for scalar quantities that enable the μ_t to be calculated. Two-equation eddy-viscosity turbulence models, despite their limitations, provide solutions with reasonable accuracy and low computational cost. There are several eddy viscosity models, but only the k-ε turbulence model will be presented here.

$k-\varepsilon$ Turbulence Model

The k-ε turbulence model is a widely used to simulate the mean flow characteristics of turbulent flow conditions. It is part of the eddy viscosity models, which aim to model all turbulence effects. k-ε model is a two-equation model, meaning it solves two transport equations besides the conservation equations. These equations consider the convection and diffusion of turbulent energy, and the two transported variables are turbulent kinetic energy (k) and turbulent dissipation rate (ε) (24). The turbulent kinetic energy determines the energy present in turbulence, while the turbulent dissipation rate determines the turbulent energy dissipation rate. Since the inception of the k-ε model, numerous efforts have been made to enhance the k-ε model capabilities, resulting in several versions of the model in STAR CCM+. This report will concentrate on the Realizable k-ε Two-Layer model.

The Realizable k-ε Two-Layer model merges the Realizable k-ε model with the Two-Layer methodology. The Realizable k-ε model introduces a new transport equation for the turbulent dissipation rate ε and applies a variable damping function f_μ to a critical coefficient of the model C_μ, which is expressed as a function of mean flow and turbulence properties. By doing so, the model satisfies certain mathematical constraints on the normal stresses, which is in line with the physics of turbulence (realizability). Furthermore, this concept of the damped C_μ approach also agrees with experimental observations in boundary layers according to STAR CCM+. As a result, the model offers substantial improvements over the other k-ε models (Standard k-ε) in many applications and generally produces results that are equally accurate or more precise (25).
Moreover, the Two-layer approach adds the flexibility of an all-y^+ wall treatment, enabling the Realizable k-ε model to be used with fine meshes to resolve the viscous sublayer. The all-y^+ wall treatment combines features of the high-wall treatment for coarse meshes and the low-y^+ wall treatment for fine meshes. It is also designed to provide accurate results for meshes of moderate resolution. Additionally, The Realizable k-ε model has an immediate advantage in that it more precisely forecasts the spread rate of planar and round jets. It is also expected to provide better results for flows with rotation, boundary layers exposed to strong adverse pressure gradients, separation, and recirculation (25). To conclude, the Realizable k-ε Two-Layer model is preferred because it can offer precise outcomes in recirculation (swirling) flows without the need for a fine mesh close to the walls. For more detailed descriptions and equations of the Eddy viscosity models, see (25)- (26) and (21).

2.6 Multiphase Flow

Multiphase flow is the simultaneous flow of either two materials with different chemical properties or one material in multiple states or phases. This is common in combustion processes, where liquid fuel evaporates before combustion. The challenge in modeling multiphase flow is the presence of fluid interfaces, which must account for varying material properties and the transfer of mass, momentum, and energy. In addition, it is often unfeasible or impossible to calculate a device's full size in multiphase processes due to substantial differences in physical scales between the phases. The multiphase flow modeling method can be through an Eulerian or a Lagrangian technique.

The Eulerian Multiphase (EMP) model calculates the balance of mass, momentum, and energy for each of the separate phases present in a system by focusing on a specified frame in space. The model uses phase interaction models to describe the effects of one phase on another, considering the interfacial area between the two phases. These phase interaction models define how energy, mass, and momentum are exchanged between the two phases, providing a completer and more accurate picture of the system being studied. In addition, it resolves the transport equations for mass, momentum, and energy of each phase, with all phases having a shared pressure field.

The Lagrangian Multiphase model is a technique that focuses on tracking individual, representative particles of the dispersed phase as they move throughout the system. This model is particularly useful when the system mainly consists of a continuous phase with a smaller volume of discrete particles, droplets, or bubbles. It is particularly effective when the interactions of the discrete phase with physical boundaries play a significant role in the system's overall behavior. Furthermore, the trajectory of each particle can be determined through this method. In the case of flows with a limited number of dispersed particles, it is possible to calculate their paths by solving a set of Lagrangian equations for each particle. However, a statistical approach is more feasible when the number of particles is substantial. In this approach, the entire population of particles is represented by a smaller number of computational parcels, reducing the computational cost. Each of the parcels stands for a cluster of particles with similar properties. Therefore, it is crucial to ensure that each parcel contains enough particles to represent the properties of the entire population accurately and that a sufficient number of parcels are used in the simulation to represent the properties of the entire particle population. In equation (11) the Lagrangian framework is used to write the momentum conservation equation for a particle. The alteration in momentum is equalized by the combination of resultant surface force $\mathbf{F}_s$ and body forces $\mathbf{F}_b$ that affect the particle (26).

$$m_p \frac{d\mathbf{v_p}}{dt} = \mathbf{F}_s + \mathbf{F}_b \tag{11}$$

2.7 Spray and Droplet

Spray modeling is a branch of discrete-phase particle modeling that deals with the transformation of a liquid into droplets. Many industrial processes, such as liquid-fueled combustion, rely on converting liquid into vapor. Liquid fuels have several benefits, including ease of transportation and storage, but to be used in an engine, they need to be mixed with an oxidizer in a gaseous state. To achieve this, the liquid is transformed into a vapor, promoting gas mixing.

There are two subcategories of spray modeling: primary and secondary atomization (27). Primary atomization involves making assumptions about the physics inside the nozzle to calculate the initial droplet size close to the nozzle. Moreover, Primary atomization describes the conversion of liquid into a fine spray of droplets by pressurizing it and forcing it through a small opening. The velocity at which the liquid exits the nozzle, known as the injection velocity, is a crucial factor in spray modeling. It plays a significant role in determining the atomization and break-up process, the depth of the spray, the transfer of properties between phases, and the interactions between droplets and the walls.

Secondary atomization focuses on modeling the behavior of droplets that travel through the domain and become hydrodynamically unstable, breaking into smaller droplets under the action of non-uniform surface forces. The droplets can also interact with each other through collisions, leading to the formation of larger droplets and affecting the dynamics of the spray plume (26). The way droplets break up varies based on the interplay between surface and viscous forces, as determined by the Weber and Ohnesorge numbers outlined in equations (12)

and (13), respectively. These numbers quantify the forces acting on droplets and specify the regime in which they break apart (26)- (28).

$$We = \frac{\rho v^2 D_p}{\sigma} \tag{12}$$

$$Oh = \frac{\mu}{\sqrt{\rho D_p \sigma}} \tag{13}$$

In equations (12) and (13), ρ is density, μ viscosity, v is the velocity, D_p is the droplet diameter, and σ the droplet's surface tension.

In STAR CCM+, there are 4 types of secondary break-up models available depending on the break-up regime, which is characterized by the shape of the deforming droplets (26). In this thesis, the Stochastic Secondary Droplet (SSD) break-up model will be used, which models the breakup of the droplet as a catastrophic and random process unrelated to the original droplet size, as shown in Figure 6. The particles for SSD break-up model break under three conditions: the particle's radius is greater than the critical radius determined by local droplet conditions, the *We* number is higher than the critical *We* number set in the interface, and the particle's local time or accumulated residence time exceeds the break-up time. Furthermore, the model monitors parcels moving through the domain and compares their residence time with the locally assessed break-up time. Residence time is calculated only for parcels that meet certain criteria, including a critical radius and a critical *We* number. When the particle breaks up, the new parcel's local time is reset. The Target Count and Maximum Child Parcels properties regulate the average number of particles per child parcel and the maximum number of child parcels created in each break-up event. The model employs these values to calculate the size, number of parcels, and particles per parcel (parcel count) of the child parcels, providing some control over the spray's discretization.

This SSD break-up model differs from other break-up models in three ways. Firstly, after the break-up event, the parent drop no longer exists. As a result, the particle numbering system re-numbers of particles after the event, and two particles with the same number before and after the event are not the same particle. Secondly, because the model utilizes a user-specified particle count, it rarely results in large particle counts that can be challenging to manage numerically. Finally, the break-up distribution function for SSD break-up model is a function of local conditions and is not heavily reliant on the parent's diameter. While the distribution is restricted to the range between the current and half the critical radius, the *We* number, a function of local flow, influences the function more strongly. For a more detailed understanding of spray and droplet modeling in STAR CCM+, see (26).

Figure 6: Catastrophic break-up of a droplet We>100 (26)

2.8 Species Transport

The composition of a multi-component gas or liquid mixture, modeled through its species, affects the fluid's overall physical properties, such as its density and molecular transport

properties, as well as its ability to absorb, based on its mass fraction. Therefore, additional transport equations are solved for the simulation of multi-species flow. This is because the distinct material properties of each species necessitate the calculation of their mass fraction in the mixture. Therefore, equation (14) is used to determine the transport equation for each species, which takes into consideration the mass fraction (Y_i) and the source term for chemical processes (S_{Y_i}) for each individual species.

$$\frac{d}{dt}\rho Y_i + \nabla \rho Y_i \mathbf{v} = \nabla \cdot \left(\rho D_{i,m} \nabla Y_i + \frac{\mu_t}{\sigma_t} \nabla Y_i\right) + S_{Y_i} \tag{14}$$

The term $\rho D_{i,m} \nabla Y_i$ is used to calculating laminar diffusion, where $D_{i,m}$ is the molecular diffusivity. On the other hand, the calculation for turbulent diffusion, which is the transport of a substance or property, involves the term $\frac{\mu_t}{\sigma_t} \nabla Y_i$, where μ_t is the turbulent dynamic viscosity, and σ_t is the turbulent Schmidt number (26).

2.9 Reacting Flow Modelling

Different chemical substances mix and react when the chemical conditions are favorable in reacting flows. STAR-CCM+ integrates species and energy transport equations with chemistry solvers to simulate these flows to calculate the source terms. STAR-CCM+ divides reacting flow models into two types: the reacting species transport and flamelet models (26).

Reacting Species Transport Models

The reacting species transport models involve solving the conservation equations, including the chemical source term, for all species in the mechanism. This method is suitable for reacting flow systems where the mixing timescale is shorter than the reaction timescale of one or more species and can be applied to simulate the slow formation of pollutants, part-load combustion scenarios, and transient combustion events such as explosions, ignition, and extinction. Various reacting species transport models are available in STAR CCM+; however, the complex chemistry model will be used here.

The Complex Chemistry model uses chemical mechanisms containing tens or hundreds of species and thousands of reactions in either the gas-phase or liquid phase. Because of the varying rates at which different species evolve, the kinetics are considered stiff (reaction systems with a wide range of reaction time scales) and integrating the reaction step is computationally expensive. To address this issue, the model employs a stiff solver to integrate the chemistry over a time-step, and one of the techniques used to speed up calculations is clustering, which groups cells with similar thermal and chemical states before integrating the averaged state for the group. This method provides a substantial speed-up, as the number of clusters is less than the number of cells in the simulation, and clustering performance improves with mesh size. Moreover, the model requires detailed reaction mechanism information about species, reactions, thermodynamics, and transport properties, which are supplied by complex chemistry definition files imported in the Chemkin format.

Furthermore, the Complex Chemistry model offers a general approach to modeling finite-rate kinetics, which can be used when other models do not capture the finite-rate effects that drive the process. It also includes sub-models for simulating turbulence-chemistry interactions, such as the Laminar Flame Concept (LFC) or the Eddy Dissipation Concept (EDC). The LFC model evaluates the instantaneous reaction rate at the mean temperature, pressure, and species mass fraction, making it appropriate for premixed, partially premixed, and unsteady flames. For more about reacting species transport models, see (26).

Flamelet Models

On the other hand, the flamelet models characterize the reacting flow system using a limited number of flamelet variables that describe the thermochemical state in the CFD cell. Instead of solving the conservation equations for all species, the conservation equations are solved for the limited flamelet variables, resulting in reduced computational cost. The specific flamelet model determines the number and type of flamelet variables that need to be solved. The flamelet approach is appropriate for reacting flow systems where the reaction timescale is shorter than the mixing timescale and is useful for simulating steady-burning furnaces, burners, and full-load combustion conditions. The flamelet method has several drawbacks, including its inability to account for the impact of the three-dimensionality of the flow field (convection and diffusion) on the flame structure, the decoupling of chemistry and transport, and the failure to capture the most intricate chemistry-turbulence interactions (19). However, its greatest advantage lies in its computational efficiency. Although the flamelet model may be appropriate for the thermal flame structure in strongly 3D flows, such as swirling flows, it is not suitable for the velocity field (19). There are three different flamelet models in STAR CCM+, the Chemical Equilibrium (CE) model, the Steady Laminar Flamelet (SLF) model, and the Flamelet Generated Manifold (FGM) model.

The CE and SLF models are restricted to simulating fast chemical reactions without ignition and extinction, whereas the FGM model can be applied to any combustor. The FGM model is considered to be the most precise among the flamelet models, according to the simulation software STAR CCM+ (26). The combustion process occurs in a thin layer that separates unburned and fully burned mixtures. A special tracking variable is introduced in each cell to monitor the combustion layer, which enables the solution of a transport equation that follows the mixture's progress as it transitions from unburned to fully burned. This progress variable, represented by c in equation (15), has a value of zero for unburned conditions, 1 for fully burned conditions, and a value between zero and 1 for partially burned fuel.

$$\frac{\partial}{\partial t}(\rho c) + \nabla(\rho \mathbf{v} c) - \nabla(\Gamma_c \nabla_c) = \dot{\omega}_c \tag{15}$$

The mixture density is represented by ρ, the diffusion coefficient by Γ_c, which includes laminar and turbulent contributions, and the source term $\dot{\omega}_c$, calculated based on the context in which c is solved. Flamelets are approximated as laminar structures. A statistically independent probability density function (PDF) can be used for the progress variable c and the heat loss ratio γ to simulate a more turbulent behavior. The composition PDF method involves solving a modelled PDF transport equation to compute the joint PDF of the thermochemical state of a mixture in a turbulent flame over time and position (19). The composition variables used are typically the mass fractions of all relevant chemical species, along with the mixture-specific enthalpy. By using these composition variables, one can calculate the chemical reaction rates and thermodynamic properties, such as the mixture density and temperature (19). Moreover, an ignition process is required to initiate combustion, and in the FGM model, this is achieved by defining a region where the progress variable changes to c=1 for burned fuel. For a more detailed understanding of how this is implemented in STAR CCM+, see (26).

The fluid streams for a reacting flow can be defined in the flamelet table generators, with the option to have either two or three streams consisting of oxidizer, fuel, and a third stream. The FGM table must be regenerated when a third stream is introduced into the computational domain since it participates in chemical reactions. Each stream is characterized by its fluid stream components, composition specification, and temperature. Additionally, an inert stream can be defined using the Inert Stream model within the FGM framework (26).

2.9.1 Inert stream

The Inert Stream feature in START CCM+ allows for including a stream of inactive flow alongside fuel and oxidizer streams in simulations. This feature allows users to specify the inert stream species separately, avoiding unnecessary computations. Unlike a secondary mixture fraction (third stream), the inert stream does not undergo chemical reactions with the fuel and oxidizer, and its composition remains the same after mixing. However, it still affects the simulation by influencing the enthalpy, specific heat, and density of the mixture, as well as diluting the overall mixture and impacting the mixture fraction properties. The transport equations for the mixture fraction consider the fraction of the inert stream and the fraction of the active fuel stream at each inlet. The Inert Stream model presumes that the inert flow and reacting flamelet species are in thermal equilibrium (26).

2.10 Injectors and Particle Distribution

In STAR-CCM+, injectors are utilized to introduce particles into the fluid continuum. The injector determines particle injection's location, direction, and frequency, while the SSD break-up model governs the particle's behaviour and break up within the domain. Several injector types are available within STAR-CCM+, and for this specific project, the solid cone injector is the most appropriate. This type of injector introduces particles from a single point, with only the outer angle of the cone needing to be specified. Additionally, the injection points of the solid cone injector serve as the initial particle positions. Next, the specified number of parcel streams is injected in random directions, following a uniform distribution on the surface of the cone. Once the direction is established, the specified velocity magnitude determines the velocity.

Moreover, there are various distribution functions available for the injector in STAR-CCM+. For this project, the Rosin-Rammler size distribution function is utilized. This function is a smooth and continuous distribution that relies on four parameters: reference size, exponent, minimum size, and maximum size. Its purpose is to describe the volume distribution of particles as a function of their diameter, $F_V(D_p)$ presented in equation (16). The parameters in equation (16) are the exponent q and the reference size of the droplet D_{ref}.

$$F(D) = 1 - \exp\left[-\left(\frac{D}{D_{ref}}\right)^q\right] \tag{16}$$

2.11 Comparison Data

The flame shape and velocity contour plot of SCM will be compared with the research of D. Moëll et al., who performed Unsteady Reynolds Averaged Navier-Stokes (URANS) simulation using ANSYS CFX 14.5 on the complete model of the SGT-800 combustor (17). D. Moëll et al. investigated three different mixtures of hydrogen with methane, including the flame shape, flame position, vorticity, and global pressure drop. The numerical data from this report, according to SE, is in good agreement with the experimental data. Therefore, the SCM's flame shape and vorticity contour can be compared with D. Moëll et al work. However, one needs to remember that the comparison will be with URANS simulation which are time averaged for flame shape and instantaneous magnitude of vorticity field for the SST turbulence model. The main goal of this comparison is to conclude how the physical phenomena such flame shape and

vorticity of the simplified combustor model behave in relation to theory and research of D. Moëll et al (17).

Furthermore, Numerical results of the flame temperature at the outlet of the SCM from CFD simulations will be compared with in-house calculations provided by SE. In-house calculations are performed using an excel sheet. The in-house calculations are not valid for emulsion (diesel & water mixture) and Methane + vapor cases, it is only valid when fuel and water are injected separately. Furthermore, for in-house calculation diesel fuel is defined as 86.4 % Carbon, 13.3 % Hydrogen and 0.4 % Sulfur, and gas fuel as 100 % CH_4. Water temperature can vary between 15 to 210 °C and gas fuel temperature can vary between 15 to 240 °C. Diesel fuel temperature can vary between 15 to 100 °C as input parameter. Moreover, the in-house calculation sheet has been verified for liquid and gas fuels as well as for water injection. After validating it with the SE in-house code so called GTPerform data , it was discovered that the in-house calculation sheet overestimates the outlet temperature of the combustion chamber by 0.25-0.5%. According to SE, the primary cause of this error in the in-house calculations is the application of thermochemical databases (collection of thermodynamic and kinetic data for various chemical species), reaction mechanisms, rounding errors in specific heat coefficients, as well as fuel temperature and air composition. The author of this thesis did not pursue further investigations into the in-house calculation sheet due to time constraints, project scope, and lack of experience in the field of combustion. However, it is vital to consider these limitations when drawing conclusions.

Moreover, it is possible to compare the CFD results for the outlet temperature in the gas fuel case with those obtained from Cantera software. Cantera is an open-source software suite designed for addressing problems related to chemical kinetics, thermodynamics, and transport processes. It offers the capability to create objects representing different phases of matter, interfaces between these phases, reactors, 1-dimensional reacting flows, and more. With Cantera, one can perform calculations for chemical equilibriums, simulate autoignition, or analyse the propagation of 1-dimensional flames, among other applications. While the majority of the program is implemented in C++, it also provides interfaces for other languages such as Python, MATLAB, and Fortran 90/95. In the context of this thesis, the Cantera calculations will be conducted by SE (presumably a colleague or collaborator) and the author will not be directly involved in the calculations or deeply explore the limitations of Cantera. For further information about Cantera see, (29).

3. Methodology

This chapter will provide an overview of the process used to create the models, starting with the initial geometry and ending with the simulation of the CFD model in STAR CCM+. Then, the focus will be on explaining the steps to arrange the models.

3.1 Workflow for Generating CFD Model

The process of conducting a CFD analysis begins with establishing the computational domain. In this thesis, STAR CCM+ is used as the simulation software. This program provides a convenient single interface solution, making it possible to create a new Computer-Aided Design (CAD) file or import an existing one. This streamlines the process and makes generating the necessary computational domain easier. Later on in this thesis, the following subsections will be described in greater detail along with an explanation of how they were achieved.

3.1.1 Cad-cleaning

The first step in conducting a CFD project is to generate the fluid domain that is being studied. This is accomplished by using existing CAD geometries. However, depending on its quality, some parts of the geometry may require further preparation or repair.
STAR CCM+ offers a 3D-CAD tool within its interface to identify errors in the geometry automatically. These errors are flagged with different colors based on the type of error and can be repaired using the surface repair tool within the software. This is essential as low-quality geometries can lead to errors throughout the simulation. Furthermore, removing small, non-critical details from the geometry can improve convergence and speed up the simulation process. In this case several CAD geometries were merged in STAR CCM+ to create the SCM. Furthermore, the surfaces of the SCM are named accordingly to the appropriate boundary conditions, making it easier to apply meshing customizations and boundary conditions later on.

3.1.2 Meshing

Before conducting a CFD simulation, creating a computational grid, commonly referred to as a mesh, is necessary. The mesh is essential to CFD calculations and significantly impacts the final result. The solution to a flow problem, such as velocity, pressure, temperature, or other parameters, is determined at nodes within each computational grid cell. The accuracy of a CFD solution is directly related to the number of cells in the grid, with a higher number of cells generally leading to better accuracy. The accuracy of the solution and the cost in terms of computer hardware and calculation time both depend on the fineness of the grid.

Optimal meshes are often non-uniform, meaning the mesh is finer in areas with large variations from point to point and coarser in regions with relatively little property change. This helps to achieve the desired balance between solution accuracy and computational cost. However, poor mesh quality can lead to inaccurate results. Therefore, areas with high gradients are critical and require a denser mesh. STAR CCM+ provides mesh generation in the same interface and offers three types of cells: polyhedral, tetrahedral, and hexahedral. More about meshing in section 3.4.

3.1.3 Pre-processing

The pre-processing stage of CFD simulation is crucial as it establishes the connection between the physics and geometry of the analyzed problem. This involves defining fluid and material properties, boundary conditions, interfaces, and turbulence models. In STAR CCM+, the geometry is divided into regions that can be modeled individually. Interfaces are needed for interacting regions, and boundary conditions are assigned at the edges. As previously stated, the surfaces of SCM boundaries are given appropriate names during the CAD cleaning process. This simplifies the task of assigning the correct boundary conditions and mesh requirements. Fluid properties and turbulence and combustion models are also assigned within each region. The governing equations are then discretized and coupled within the region. STAR CCM+ offers two solver approaches, a segregated solver that solves each equation separately and a coupled solver that solves all equations simultaneously using a pseudo-time-marching approach.

3.1.4 Solver

The solver goes through iterations to find a solution by resolving the transport equations until a sufficient degree of convergence is achieved. If any convergence issues arise, relaxation factors can be applied to enhance stability, resulting in a longer computational time.

Checking for convergence during the solving process is critical. Determining when a solution has converged is often challenging, as there is no definite answer. It is a trade-off between the amount of time spent and the accuracy of the solution, and this is where engineering expertise is required. The most common method to determine convergence is to use residuals, which compare the solutions from each iteration. If the difference between iterations is small enough, the solution is considered to have converged. Additionally, monitor points are often used to track entities of interest in the solution. Results can be confidently extracted when these monitor points converge to a specific value.

3.1.5 Post-Processing

The final stage of the process involves obtaining insightful outcomes from the solver and presenting them in various forms, such as graphs, contour maps, and vector diagrams. The solution information can also be saved to external MATLAB or Microsoft Excel files for further use.

3.2 Parametric Cases

A parametric study will be conducted to investigate the ability of STAR CCM+ to predict the outlet temperature of the SCM when using liquid and gas fuels with water injection. The fuels considered are methane (CH_4) and diesel ($C_{12}H_{23}$). The study will model various cases, as shown in Table 1.

Water fuel ratio (WFR) is based on gas fuel mass flow rate, meaning that same mass flow rate of water will be added to diesel mixture as well. For the parametric cases involving water injection, the mass flow rate of water will be 0.003981995 [kg/s] which is (WFR=0.5) 50 % of total mass flow rate of methane with a temperature of 15 °C. For vapor, the temperature will

be set to the same as the warm air temperature of. In premixed cases, fuel and air will be mixed before inserting into the computational domain, and a mixture fraction must be defined at the inlet. In non-premixed cases, fuel and oxidizer streams will be inserted separately from two different inlets, explained in section 3.3. In STAR CCM+, the mixture fraction is the elemental mass fraction originating from the fuel stream. It is a conserved scalar that ranges between 0 and 1, with a value of 1 for the fuel stream and 0 for the oxidizer (air) stream. Equation (17) defines mixture fraction Z, which is the sum of the mass of all elements derived from the fuel stream (either Diesel or Methane) denoted by m_f, and the total mass of all elements that come from the oxidizer stream (air), denoted by m_{ox}.

$$Z = \frac{m_f}{m_f + m_{ox}} \tag{17}$$

Methane + Vapor + Air case fuel will be defined as a mixture of vapor(H20) and methane before generating the FGM table explained in section 3.5. Furthermore, for simplicity of the simulations, all fuel will be inserted through the main inlet, and the pilot inlet will be defined as a wall for the Methane + Vapor + Air case. More about boundary conditions in the next section.
Diesel fuel will only be modelled as non-premixed (fuel and air are not premixed). However, in the emulsion case (case 8), diesel and water will be premixed to form a fuel consisting of water and diesel. Additionally, the total mass flow rate of fuel for cases 1 and 6 will be adjusted to yield the same outlet temperature of the SCM. A more detailed description of boundary conditions and how combustion, spray (water injection), and certain cases are modelled in STAR CCM+ is described in later sections.

Table 1: Parametric cases with Water/Vapor and total fuel mass flow rate is presented.

CASE Nr	Type	Case Name	Water/Vapor Mass flow Rate [Kg/s]	Total Fuel Mass flow Rate [Kg/s]
1	Fuel-air-Premixed	Methane + Air		0.007964
2	Fuel-air-Premixed	Methane+ Air+Water	0.00398	0.007964
3	Fuel-air-Premixed	Methane+ Vapor + Air	0.00398	0.007964
4	Non-premixed	Methane + Air		0.007964
5	Non-premixed	Methane + Air+ Water	0.00398	0.007964
6	Non-premixed	Diesel + Air		0.008955574
7	Non-premixed	Diesel + Water+ air	0.00398	0.008955574
8	Non-premixed	Emulsion (Diesel & Water mixture) + Air	0.00398	0.008955574

3.3 Geometry Simplification and Boundary Conditions

Geometry simplification is essential to reduce the computational cost of simulations without affecting their accuracy. Figure 8 illustrates the complete geometry of the SGT-800 gas turbine combustor from Siemens Energy, with the simplified combustor area outlined in red. The SGT-800 gas turbine consists of 30 combustors, each with 12 pilot fuel inlets. However, its large computational domain makes simulating the entire SE combustor complex and computationally expensive.

Therefore, SCM will be used for fast turnaround and good convergence. The SCM is a 30-degree cut of one burner and its coordinate origin is at the outlet of the mixing tube, as presented in Figure 9. Moreover, the SCM domain starts after the swirl cone outlet and end at the guide van of the turbine. It is consisted of a 30-degree mixing tube sector, one pilot fuel inlet, and combustor chamber walls. The number of inlets for a simplified combustor model depends on the type of the simulation case. For premix cases, only two inlets are required, one for premix air-fuel called main inlet and the other for pilot fuel inlet, situated in the burner tip close to the combustion chamber, shown by the blue circle in Figure 9. For each inlet, a specific mass flow, temperature, velocity magnitude, and mixture fraction need to be defined. In this project, 95% of the total fuel mass flow rate is through the main fuel inlet, and 5% is through the pilot fuel inlet. The SCM outlet is situated downstream of the combustion chamber contraction, which is a zero gradient pressure outlet. All walls are treated as no-slip adiabatic walls and rotational periodic boundary conditions are applied for periodic interface since only a 30-degree of the entire SGT-800 combustion chamber is modeled.
Figure 8 shows that the SCM main inlet starts after the swirling cone. As described in section 2.1, the swirl cone creates a swirl that improves the mixing of air and fuel. Therefore, the velocity vector component (swirl profile) will be taken from the global model (entire STG-800 combustor model), which describes the flow direction after the swirl cone in axial and tangential direction shown in Figure 7. SE provides the velocity profile table and describes tangential and axial directions for the main inlet mass flow rate as a function of main inlet radius. Figure 7 shows the normalization of axial and tangential velocity by the maximum velocity, as well as the normalization of radius by the maximum radius of the mixing tube.

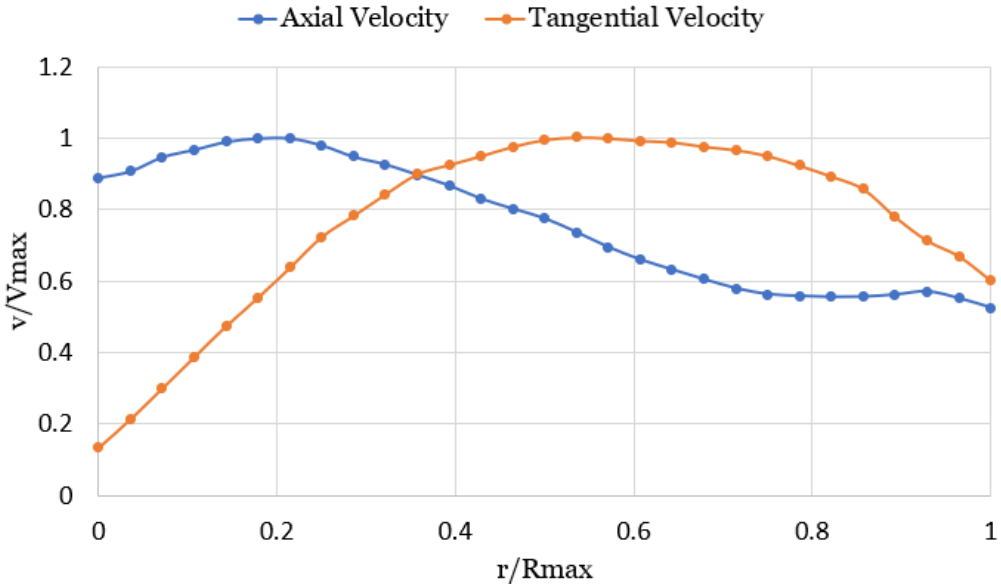

Figure 7: Velocity profile direction component in axial and tangential directions after swirling cone of SGT-800 combustor.

On the other hand, for non-premix cases, the main inlet is split into two regions, fuel and air will be inserted through different inlets, as shown in Figure 9. However, obtaining converge and reasonable simulation results for the SCM was not straightforward. In the initial stage of the project, other models have also been tested, which gave unrealistic results and caused divergence; for more details, see Appendix A.1.

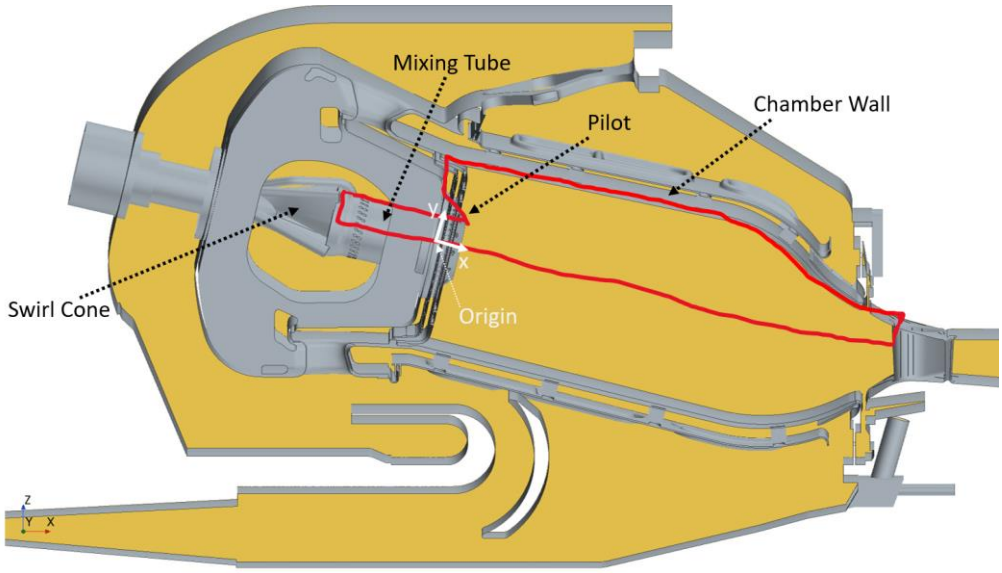

Figure 8: Entire SGT-800 gas turbine combustor where red lines represent the simplified model.

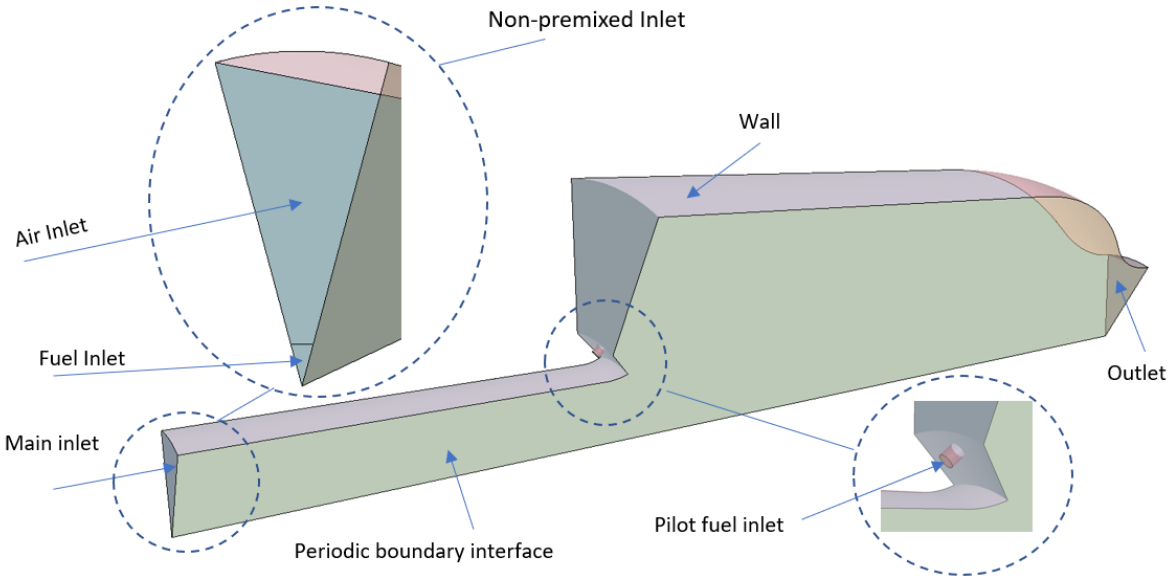

Figure 9: Simplified combustor model (SCM) geometry

3.4 Meshing and Mesh Verification

The 3D-CAD tool within STAR CCM+ was used to import the CAD geometry of the fluid domain. This allowed for naming all faces in 3D-CAD, which facilitated the implementation of boundary conditions. Additionally, the tool made surface meshing possible, enabling the assignment of varying target cell sizes to the geometry surfaces. A cross-section of the simplified combustion chamber is seen in Figure 10a, along with the mesh distribution. The highest density is seen inside the mixing tube and the flame region close to the burner tip. The flow is very complex, and the highest gradient is expected in that region of the computational domain.

Moreover, prism layers are commonly utilized near the wall to model the near-wall boundary layer precisely. These cells are typically hexahedral and combined with the chosen cell type as they move further from the wall. Furthermore, the shape of the mesh elements plays a crucial role in affecting numerical diffusion, quality, and computational time. Therefore, polyhedral cell elements were used for meshing the SCM with prism layers being utilized to model the near wall as shown in Figure 10b. The polyhedral mesh is computationally efficient and suitable for multi-directional (swirling) flow (30). The numerous neighbors each cell of the polyhedral mesh has contributes to well-approximated gradients and reduced numerical diffusion caused by flows not normal to any cell face (31). Moreover, the polyhedral mesh can handle simple and complex geometries, providing better control over mesh refinement areas.

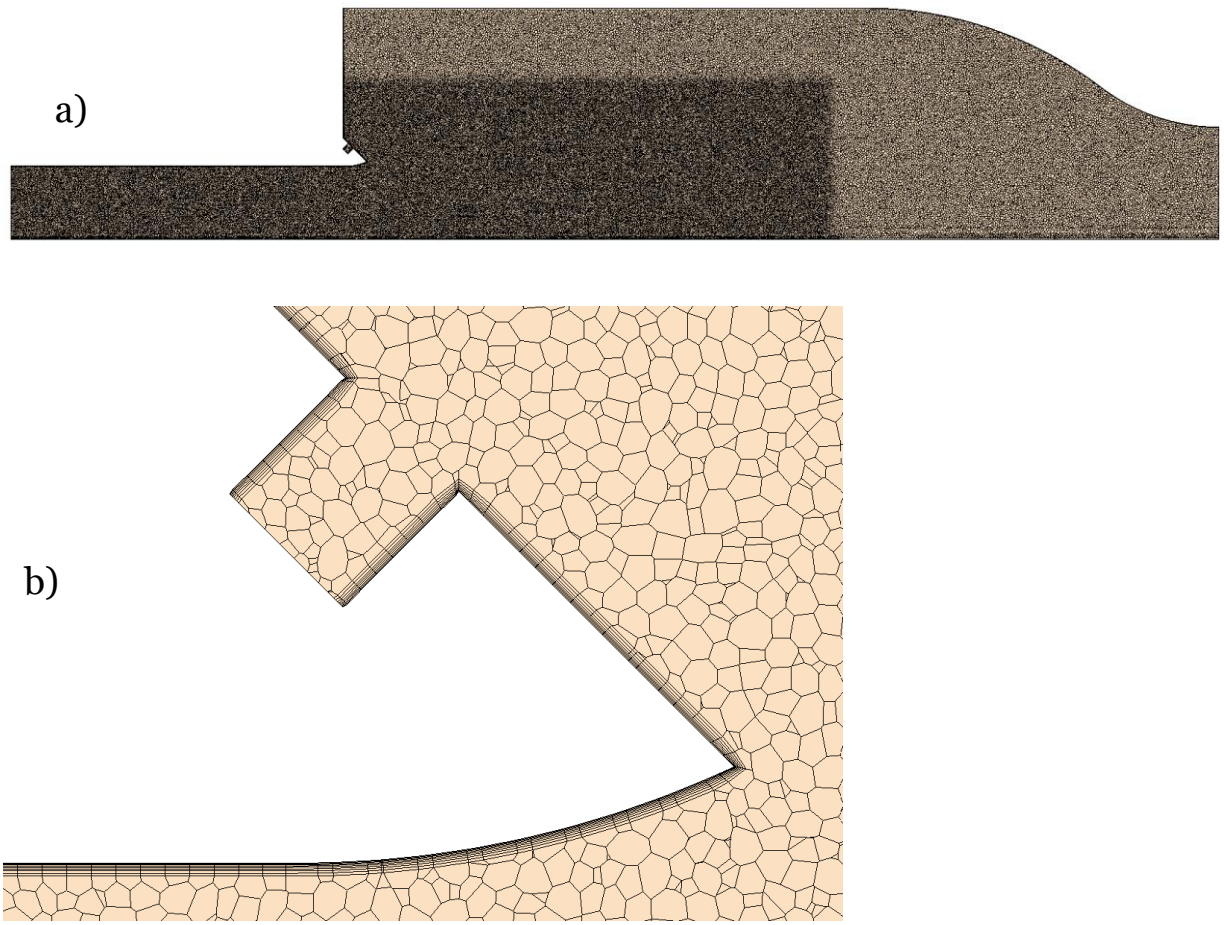

Figure 10: a) cross-section of the mesh used for parametric study of the simplified combustor model. The mixing tube region and the area close to the burner tip is refined. b) Prism layers close to the wall and pilot fuel area are zoomed in.

A mesh verification study is carried out on a simplified combustor model for a premixed Methane + air with water injection case. Three meshes is used, with varying numbers of cells - coarse, medium, and fine. The outlet temperature of the combustor is compared between the different meshes, and the results are presented in Table 2. The difference in temperatures between the meshes decreased as the number of cells increased. The medium and fine mesh difference is only 0.01% or 0.2 °C.
Moreover, a temperature profile along a vertical line at x=0.08 m (0.08 m from the burner tip) is plotted for all meshes in Figure 11. The temperature along the y-axis for the coarse mesh diverged from the medium and fine meshes. Based on the results in Table 2 and Figure 11, it is concluded that the medium volume mesh with 2.9 million polyhedral cells and eight layers of prism layers, and maximum cell size of 0.6 [mm] in the refinement region provided a good balance between computational cost and accuracy.

Table 2: Mesh sensitivity for outlet temperature of the SCM.

Mesh	Num Cells	Outlet Temperature °C	Difference percentage (%)
Coarse	1439329	1433.2	
Medium	2906612	1435.1	0.13
Fine	4762685	1435.3	0.01

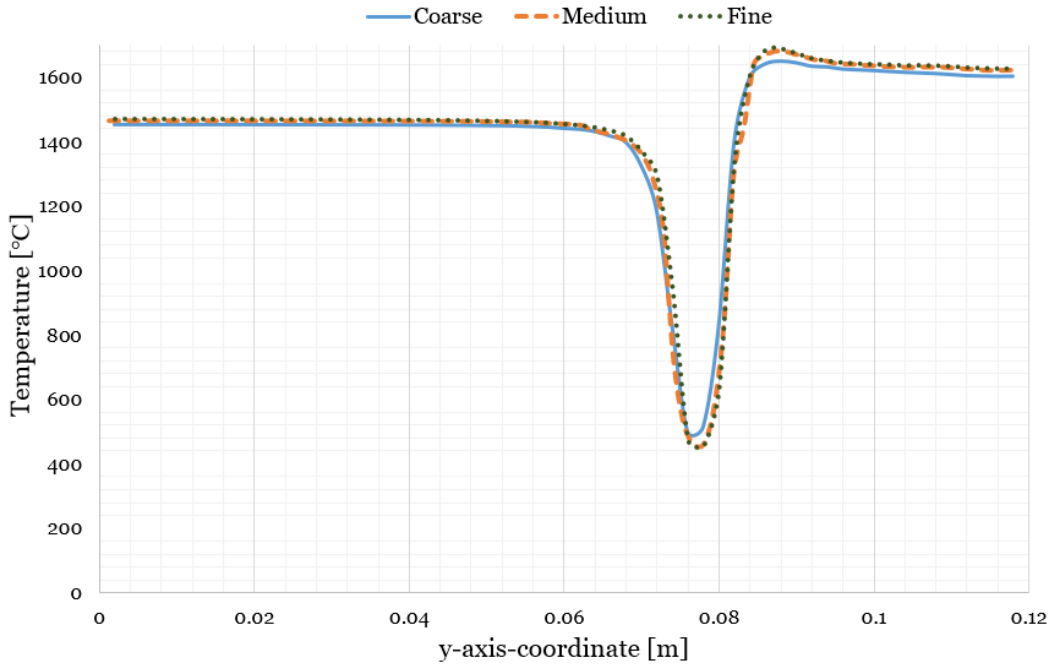

Figure 11: Temperature profile along the y-axis-coordinate at x=0.08 for three different meshes.

3.5 Combustion Implementation

As described in section 2.9 in STAR CCM+, different reacting flow models are available for modeling the combustion process inside the SCM. During this thesis, the FGM model has been mainly used for modeling combustion. This model is considered the most precise among flamelet models and is computationally cheap according to STAR CCM+ (26). The FGM model determines the thermodynamic and transport properties of the fuel and oxidizer by referring to Chemkin files. These files describe the chemical reactions, thermodynamic properties, and transport properties of the species involved in the combustion process. To generate the FGM table, three separate Chemkin files are required. The first one is the Chemistry Reaction file which contains chemistry reactions that outline how molecules interact. The second file contains thermodynamic properties that describe the thermal characteristics of the different compositions. Lastly, the third file includes transport properties that enable STAR CCM+ to compute the mean molecular dynamic viscosity, thermal conductivity, and molecular diffusivity based on the temperature and flamelet species present. This thesis employs the GRIMech 3.0 mechanism in Chemkin format, it is a detailed kinetic mechanism developed by the Berkeley combustion team to model methane-air combustion. The mechanism consists of 325 reactions and 53 species and was initially designed as an optimized mechanism to simulate natural gas combustion. For additional details regarding the GRIMech 3.0 mechanism see (32). For modelling of diesel fuel combustion smaller kinetic mechanism Z65 is provided by SE which is consisted of 65 reactions and 24 species.

The composition of the oxidizer and fuel must also be specified. The oxidizer is set as default with 76.6% N2 and 23.3% O2, while the fuel is set to be 100% CH4 for methane and 100% DF2-C12H26 for diesel cases, requiring different Chemkin files for each fuel type. After importing the necessary files, the FGM table can be generated before running the simulation. The FGM table consists of pre-calculated chemical and transport properties of the flamelet species, which are utilized during the simulation to determine variables such as temperature and species concentrations in the flamelet regions. Moreover, complex chemistry model has been also implemented for methane fuel, more about complex chemistry see appendix A.4.

3.6 Spray Implementation

The Lagrangian method is used to model liquid injection, which involves tracking the movement of diesel and water droplets from the spray injector. Setting up this behaviour in the CFD solver involves defining the models used for the Lagrangian phase, creating injectors, and setting parameters for the Lagrangian solver.

The physical model that has been established for the Lagrangian phase provides a detailed understanding of the interaction between the injected fluid and the airflow within the combustion chamber. To ensure accuracy in the simulations, the residence time has been selected automatically for steady-state simulations. In addition, the Two-way coupling model has been chosen, which facilitates the interaction between droplets and other fluids while exchanging transport equations. The Quasi-Steady Evaporation model has been employed to enable the droplets to evaporate when they reach sufficiently high temperatures. The diesel (DF2-C12H26) droplets are designed to evaporate into C12H23 molecules that act as fuel in the combustion process. To simulate the turbulent behavior of the droplets, the turbulent dispersion model collaborates with the RANS turbulence model. The SSD secondary break-up model has been incorporated into the simulation to accurately predict the break-up of droplets when they disintegrate in the air. The drag force that acts on the droplet has been calculated using the Schiller-Naumann model, while the heat transfer has been calculated with Ranz-Marshall.

Injectors were defined as solid cones with an outer cone angle of 15 degrees. The size of the droplets that were injected into the SCM was determined by using a Rosin Rammler distribution. The reference droplet diameter was 49.6 µm, with upper and lower limits of 100 µm and 10 µm, respectively. The injector velocity at the main inlet was set to 100 m/s, and each injector was initially loaded with 100 parcel streams.

For the Diesel+ air case, two injectors were employed, with one located at the main fuel inlet and the other at the pilot fuel inlet, as shown in Figure 12. When water was added to the Diesel + Air case, an additional injector was created close to the main diesel injector. Only one injector was used at the main inlet for the methane water injection. The temperature of both the diesel and water was set to 15 °C.

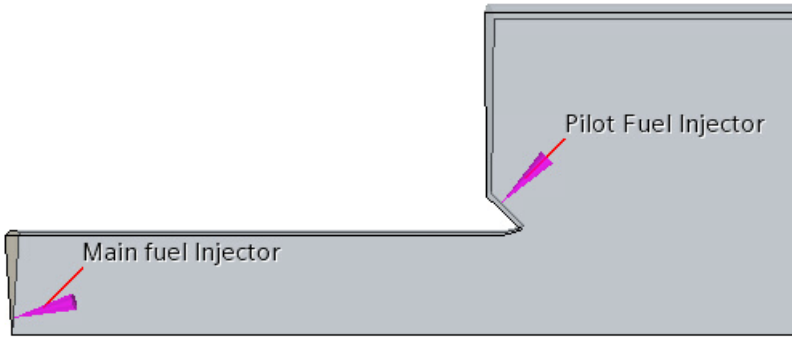

Figure 12: Injector configuration for Diesel +Air case.

Water addition to the combustion process is defined as an inert stream and as third stream. Inert stream means that water does not undergo chemical reactions with the fuel and oxidizer, and its composition remains unchanged after mixing. Nevertheless, it affects the simulation by influencing the enthalpy, specific heat, and density of the mixture, as well as diluting the overall mixture and affecting the mixture fraction properties, as described in section 2.9.1. Furthermore, when water is defined as a third stream the FGM table needs to be regenerated since water now take part of chemical reactions.

For gas component material properties is taken from the flamelet table, and for the Lagrangian phase (diesel and water), the specific heat and surface tension is defined as polynomial in T. Rest of the properties were as default and unchanged. Moreover, In the emulsion case, a multi-component material consisting of (DF2-C12H26) and (H2O) was defined for the Lagrangian liquid phase. Material properties such specific heat and surface tension of the multicomponent liquid (emulsion case) were based on Mass-Weighted Mixture and Mixture respectively. All other settings remained the same for the emulsion and diesel + air cases. The only difference is that the injector set-up now requires the mixture fraction for diesel and water because one injector is used for the main fuel inlet.

The Lagrangian solver was programmed to start after the average mass flow temperature at the outlet had stabilized. This was done to ensure that an initial flow field was established within the SCM. The relaxation factors were set to default values, and the update frequency was set to 25. This meant that the Lagrangian solver would iterate after the main solver had completed 25 iterations.

3.7 Gas Fuel Implementation

Modelling the gas fuel option for the simplified combustor model was regarding computational set-up more stable than its liquid fuel. This was due to the absence of multiple phases of fluid. The same geometry was used, thus including the same simplifications and boundary conditions. Methane was inserted through both main inlet and pilot fuel inlet without any injectors. This was done by defining the mixture fraction at these inlets to 1.0 which stands for only fuel. Furthermore, an additional ignitor was added inside the combustor which start ignition after the flow was stabilized inside SCM.

3.8 Solver set-up

The Realizable k-ε Two-Layer turbulence model is used during these simulations based on its rotational and swirling flow performance. It also provides accurate results for meshes of moderate resolution (26). The segregated solver was used to couple the transport equations, and these were discretized with the second-order scheme to achieve high accuracy. However, there are other discretization scheme available at STAR CCM+. Furthermore, only steady-state RANS simulations were performed with default under-relaxation factors.

For methane + air cases, ignition started once the mass flow average temperature at the combustor outlet stagnated. Furthermore, water was injected after ignition when the combustion had fully occurred, and the mass flow average temperature at the combustor outlet stagnated.

For the diesel+ air case, diesel was injected once the air flow field was fully developed inside the combustor, which was monitored by the mass flow average temperature at the outlet of the combustor.

3.9 Post-processing

A cross-sectional plane in the xy-plane was created through the SCM to extract contour plots for velocity, temperature, mass fraction, progress variable, and vorticity. The "Mass flow average" method was used, as specified in the report definitions, to calculate the adiabatic flame temperature at the outlet of the SCM.

4. Results

This chapter will present simulation results in the form of contour plots, line plots, and tables. The physics inside the SCM will be described, and the flame shape will be compared with D. Moëll et al.'s work for the premixed Methane + Air case. Additionally, the outlet temperature for each case will be presented. Moreover, challenges with diesel fuels and complex chemistry model are addressed in Appendix A.3 and A.4 respectively.

4.1 Characteristics of SCM and Comparison

This section showcases the CFD findings for a premixed Methane + Air case. Figure 13 illustrates a vortex breakdown at the mixing tube outlet which creates a central recirculation zone and an outer zone, as discussed in section 2.1. Notably, Figure 13 is in good agreement with Figure 4 and with theory described in (16) about swirling flow expansion in combustion system. However, it's essential to note that the presented SCM in this section only displays a half cross-section of the complete combustor.

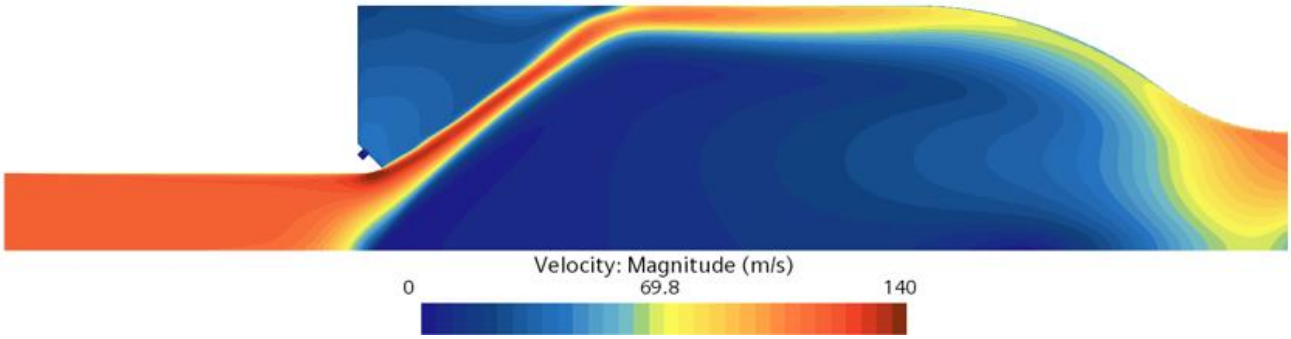

Figure 13: Velocity contour plot of SCM for Methane + Air case. The maximum velocity is inside the mixing tube and V-shaped expansion is presented at the mixing tube outlet.

Figure 14 and Figure 15 display methane mass fraction and the SCM's temperature field. For premixed methane mixture in figure 14 mass fraction of fuel (CH_4) is visible inside the mixing tube which is defined at the main inlet. The hottest temperature regions in Figure 15 are found at the pilot flames and the coldest areas are inside the mixing tube. The hottest temperature within the SCM indicates that the fuel (methane) has undergone combustion. Thus, the methane mass fraction due to combustion becomes zero at high temperatures, as seen in Figure 14 and Figure 15.

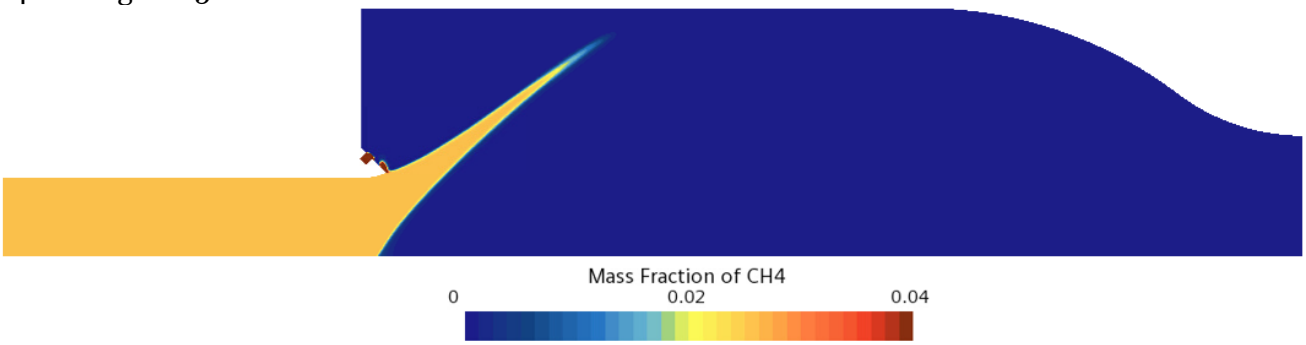

Figure 14: Mass fraction of methane for Methane + Air case in SCM. Methane mass fraction is presented inside the mixing tube and at pilot region but in the rest of the SCM Methane is fully burned.

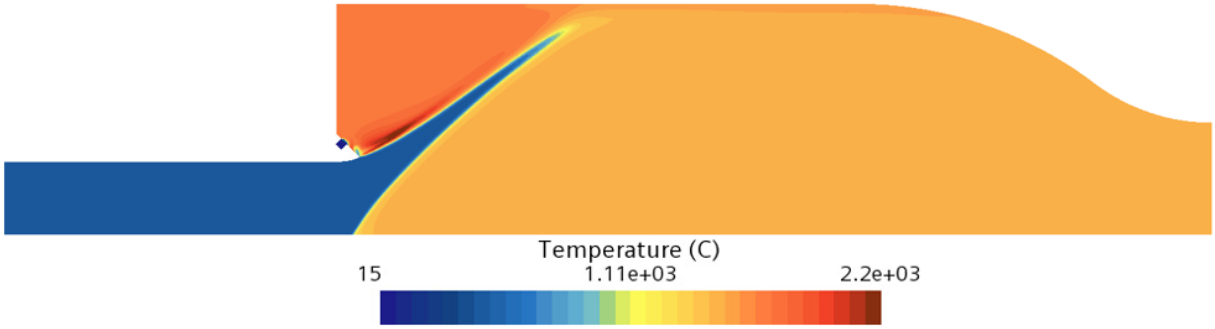

Figure 15: Temperature field inside SCM for Methane + Air case. Inside the mixing tube, there is a low temperature region while the rest of the domain presents a high temperature.

Figure 16 displays the reaction progress variable c for both SCM and D. This variable was also used in the research of D. Moëll et al. (17). The results show that the SCM closely agrees with the authors' work, as both predict a similar flame shape close to the mixing tube outlet. In Figure 16a, the fresh reactant and fully burned fuel are coloured black, while in Figure 16b, the progress variable is presented using a colour bar ranging from 0 to 1. A value of 0 represents the fresh reactant, while a value of 1 represents the fully burned products of the fuel. The resulting flame shape is in close agreement with Figure 4.

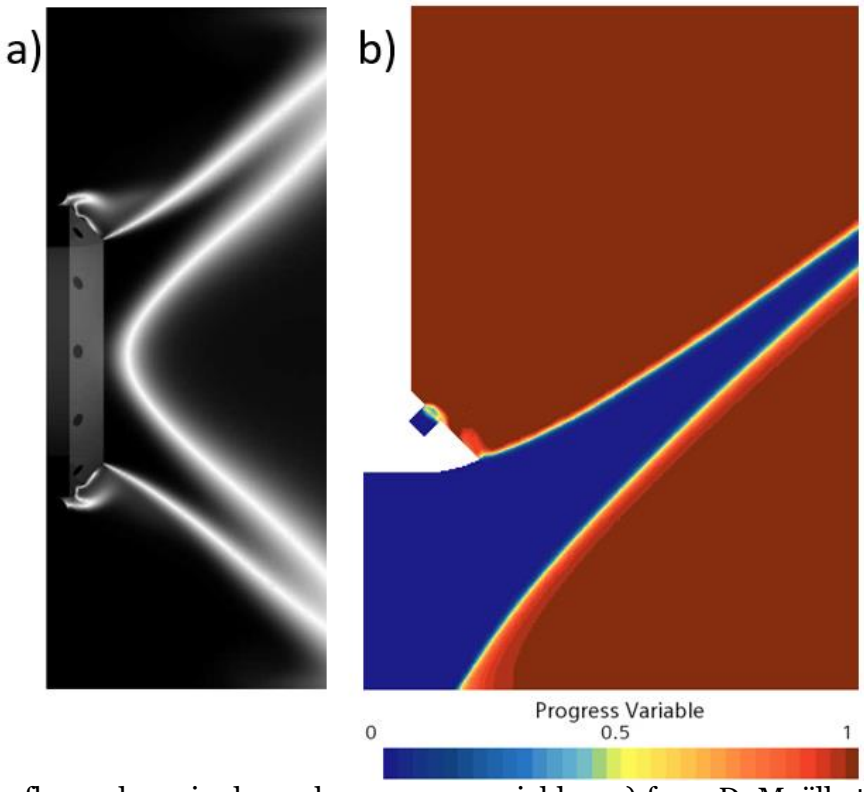

Figure 16: The flame shape is shown by progress variable c a) from D. Moëll et al. research, representing time-averaged mean flame front (17). b) Steady-state RANS flame shape of SCM.

The vorticity magnitude of the SCM was compared with the work of D. Moëll et al. (17). The highest vorticity was observed at the center of the mixing tube for both models.

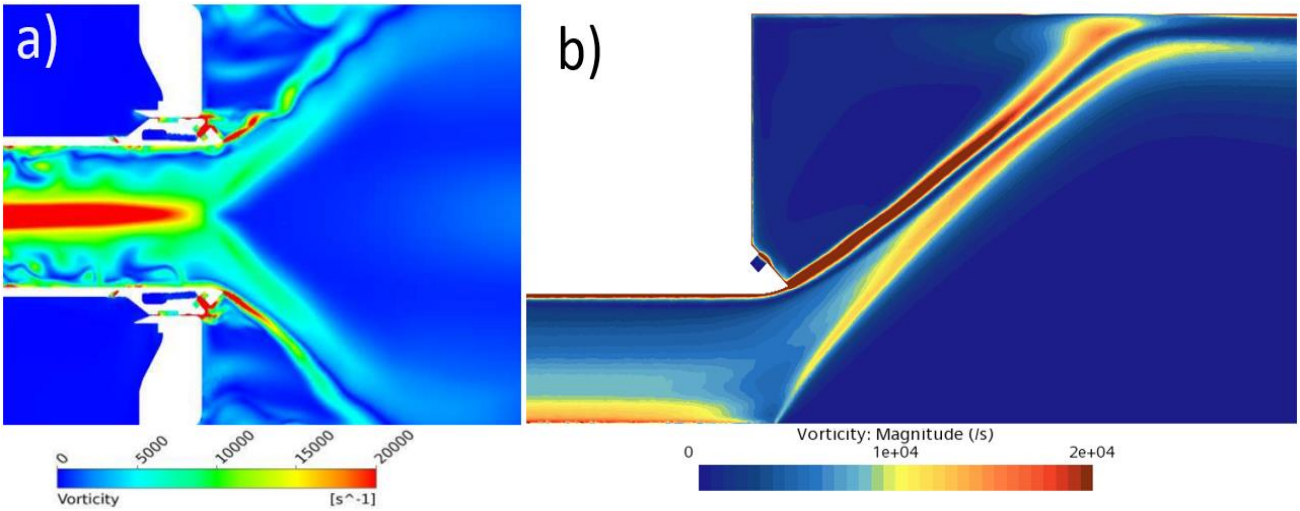

Figure 17: Vorticity contour plots. a) Instantaneous magnitude of vorticity field from D. Moëll et al. research (17). b) Steady-state RANS vorticity magnitude of SCM.

Moreover, CFD simulations indicate that non-premixed methane and diesel mixtures have unstable flame shapes and unevenly distributed temperature fields, as illustrated in Figure 17. However, the temperature field is evenly distributed when using premixed methane, as shown in Figure 15. Additionally, non-premixed Methane + Air creates a low-temperature region close to the pilot fuel inlet, whereas non-premixed Diesel + Air results in a high-temperature region.

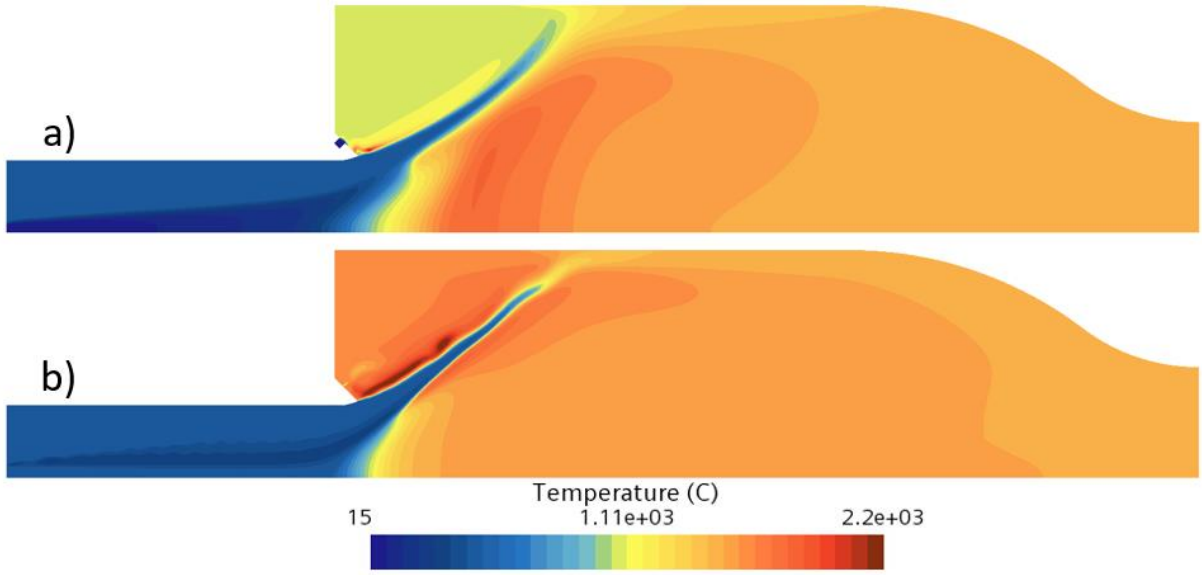

Figure 18: Temperature field distribution in xy-plane through the SCM. a) Non-premixed Methane + Air. b) Non-premixed Diesel + Air. In both cases, the flame shape appears unstable and diffuse, and the temperature distribution is non-uniform.

Figure 19a represents the contour plot for methane fuel in the non-premixed Methane + Air case, and Figure 19b for diesel fuel in the Diesel +Air case. For the non-premixed case, methane fuel is not well mixed inside the mixing tube as for the premixed Methane + Air case shown in Figure 15. Furthermore, diesel fuel evaporation is clearly visible to C12H23 which acts as fuel and the mixing is not homogenous inside the mixing tube.

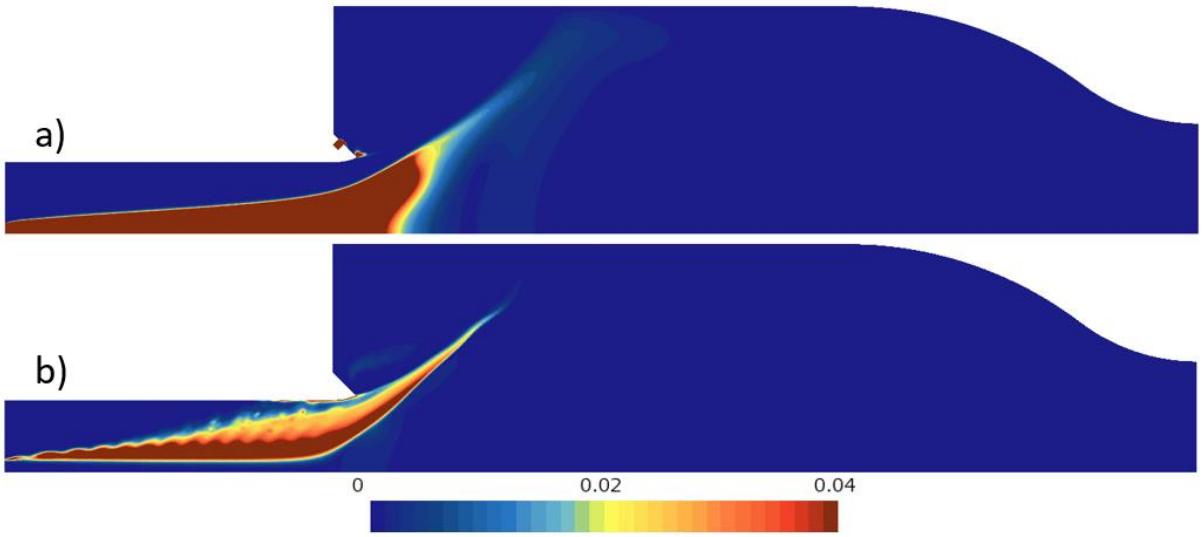

Figure 19: Mass fraction contour plot in xy-plane of through the SCM. a) Mass fraction of methane CH4 for non-premixed Methane + Air. b) Mass fraction of Diesel C12H23 for non-premixed Diesel + Air.

4.2 Comparison of Parametric Cases

The parametric cases listed in Table 1 were simulated using STAR CCM+. It was observed that the gas fuel cases exhibited smoother convergence compared to the liquid fuel cases, and the outlet temperature of the SCM temperature stagnated to values presented in Table 3. However, for diesel fuel cases, the outlet temperature fluctuated and did not settle on a specific value, as shown in Figure 20: Mass flow average outlet temperature for Diesel + Water + Air case, which shows the mass flow average temperature at the outlet of the SCM (Challenges with diesel simulations is more extensively described in appendix A.3). Therefore, the mean value of the last 5000 iterations was computed as the outlet temperature for all liquid fuel cases. Figure 20 illustrates data from the Diesel + Air case where the mass flow rate of liquid fuel has been modified during the simulation to obtain the same outlet temperature of 1475 °C as for premixed Methane + Air case.

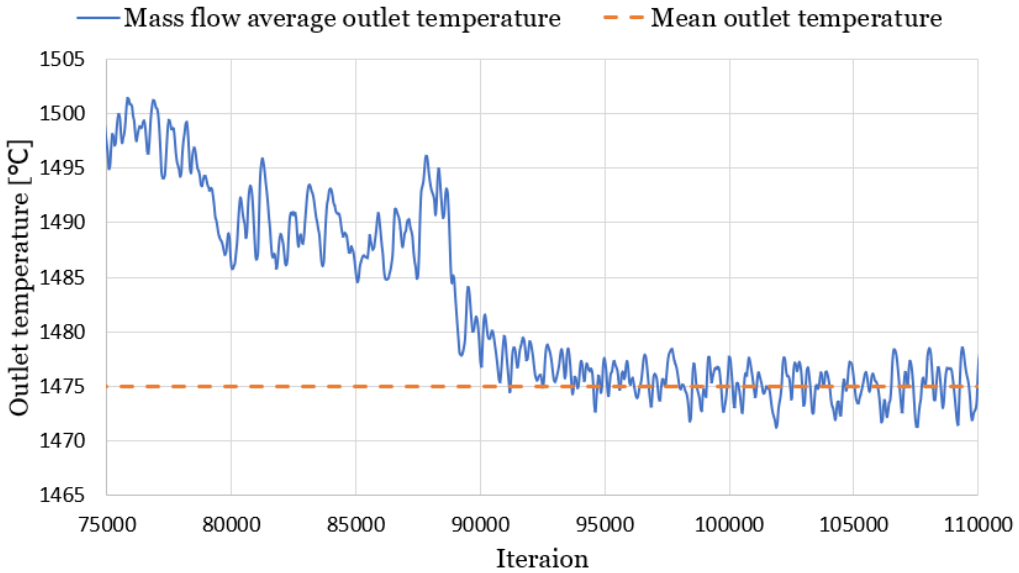

Figure 20: Mass flow average outlet temperature for Diesel + Water + Air case. (Note: The mass flow rate of Diesel was adjusted during the simulation to match the outlet temperature of the Methane+Air case. This resulted large number of iterations to reach the desired

temperature of 1475. However, the initial iterations were not included as they could affect the quality of the figure.)

The results of the CFD simulations when water is defined as an inert stream using the SCM in STAR CCM+ for all parametric cases, including in-house calculations, are presented in Table 3. Premixed Methane + Air has approximately same outlet temperature of 1474.6 °C as the non-premixed Diesel + Air case. The outlet temperature decreases when water is injected into the computational domain. For both premixed Methane + Air and Diesel + Air cases, injecting the same amount of water results in a temperature drop of 39.5 °C and 39 °C, respectively. Moreover, the non-premixed Methane + Air case does not reach the same outlet temperature as the premixed case, with a minor difference of only 1.6 °C. The temperature drops by 43 °C when water is injected into the non-premixed Methane + Air case. When water is premixed with methane as vapor, the temperature drops by 19.1 °C compared to the premixed Methane + Air case. Furthermore, when water is premixed with diesel as an emulsion mixture the temperature drop is 52.8 °C.

Table 3: CFD simulations for Inert Stream and In-house calculation results for all the parametric cases with WFR of 0.5.

CASE Nr	Type	Case Name	Outlet Temperature CFD °C	In-house caclulation °C	Cantera °C	Difference °C with In-house calc
1	Fuel-air-Premixed	Methane + Air	1474.6	1498.4	1482.9	23.8
2	Fuel-air-Premixed	Methane+ Air+Water	1435.1	1439.1		4
3	Fuel-air-Premixed	Methane+ Vapor + Air	1455.5	-	1459.6	-
4	Non-premixed	Methane + Air	1473	-		-
5	Non-premixed	Methane + Air+ Water	1430	-		-
6	Non-premixed	Diesel + Air	1475	1487.9		12.9
7	Non-premixed	Diesel + Water+ air	1436	1427.5		8.5
8	Non-premixed	Emulsion (Diesel & Water mixture) + Air	1422.2	-		-

In-house calculations are only valid for specific cases in Table 3, namely case numbers 1, 2, 6, and 7. The results obtained from in-house calculations are well aligned with CFD simulations for cases 2, 6, and 7 since these cases have a difference of less than 10 °C. For diesel cases, even though it increases the limit of 10 °C is considered good enough because diesel properties in CFD simulations and in-house calculation were not the same. Thus, a difference of 12.9 °C for Diesel + Air case is still good enough. However, water injection into the computational domain results in a greater difference between the numerical and in-house calculations. The largest difference of 23.8 °C between the in-house calculation and CFD results can be observed for premixed Methane + Air mixture. On the other hand, there is small difference between CFD and Cantera results for the premixed methane + air case and the Vapor case, with temperature differences of only 8.3 °C and 3.6 °C, respectively. It is worth noting that this difference falls within the acceptable range of 10 °C.

Moreover, Table 4 represents comparison data when water is defined as a Third Stream and Inert Stream. The outlet temperature differs approximately by 3 °C between an inert stream and third streams for methane mixtures and Diesel + Water + Air case. Furthermore, the difference between CFD and in-house calculation is increased by approximately 3 °C when water is defined as a third stream in premixed methane and non-premixed diesel mixtures. However major difference of 15.8 °C is seen in the emulsion case for these two approaches.

Table 4: Comparison of Third Stream and Inert Stream for WFR of 0.5.

Type	Case Name	Third Stream: CFD [°C]	Difference with Inert Stream [°C]	Difference with In-house Calculation [°C]
Fuel-air-Premixed	Methane+ Air+Water	1432.8	2.36	6.3
Non-premixed	Methane + Air+ Water	1433.3	3.33	
Non-premixed	Diesel + Water+ air	1438.6	2.6	11.1
Non-premixed	Emulsion	1438	15.8	

4.3 Varying Mass Flow Rate of Water

Figure 21 and Figure 22 shows how the SCM outlet temperature from CFD simulation and in-house calculations varies for varying the WFR for premixed methane + air and non-premixed diesel + air case, respectively. One should remember that WFR is based on methane fuel's total mass flow rate in both figures. In Figure 21 results from Cantera is also presented for methane cases. The SCM outlet temperature decreases as the WFR increases. The difference between in-house calculations and CFD simulations is non-linear with an increase in WFR for both type of fuels. The variance between CFD and in-house calculations for premixed methane mixture decreases from 23.8 °C to 4 °C at a WFR of 0.5. However, when comparing the results between Cantera and CFD, it is observed that the temperature difference does not exceed the limit of 10 °C for a wide range of WFR from 0 to 0.5. The smallest difference of 1.1 °C is observed at a WFR of 0.25, while the largest difference of 27.9 °C is seen at a WFR of 1.

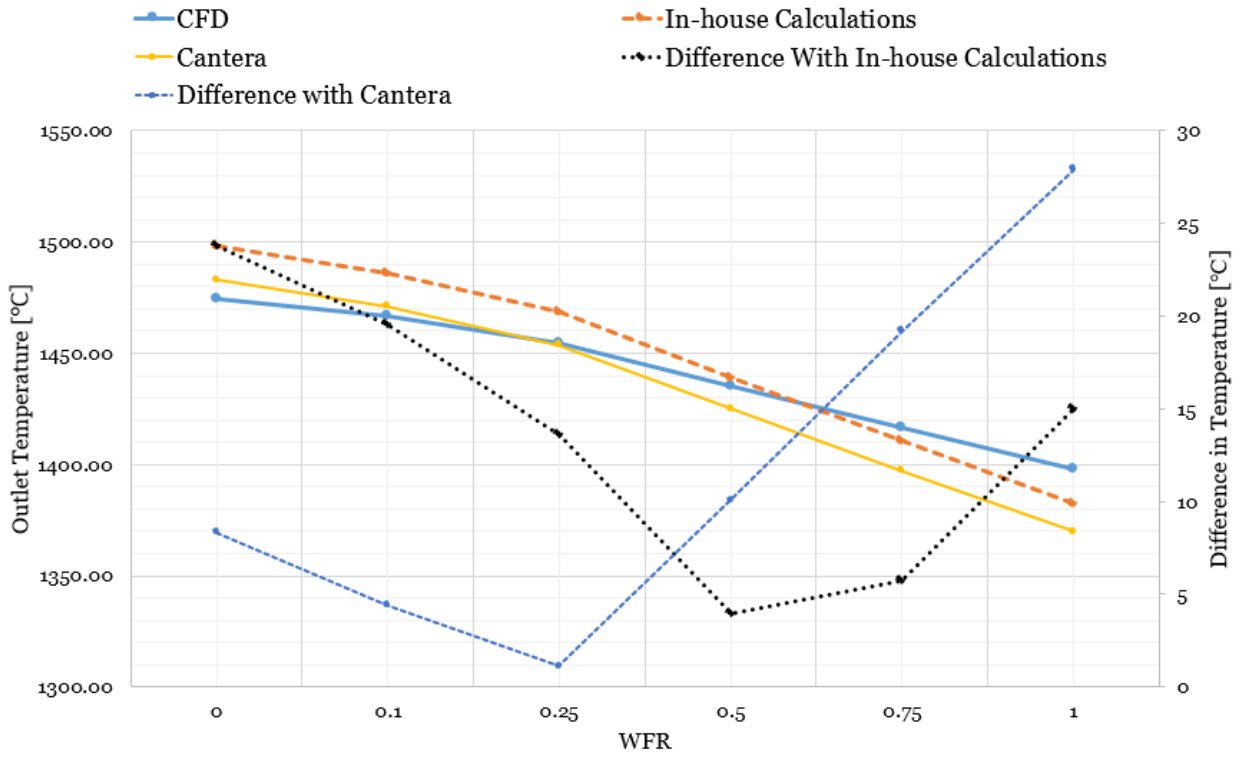

Figure 21: Comparison of CFD and In-house calculations for premixed methane + air case. SCM outlet temperature is on the left axis but on the right axis, the difference between CFD and In-house calculations is a function of WFR.

On the other hand, for non-premixed diesel + air the CFD simulations underestimates the outlet temperature for WFR less than 0.25 and overpredicting above 0.25. The minimum difference of 4 °C is observed when the WFR is 0.25 and highest difference of 28 °C for WFR of 1.

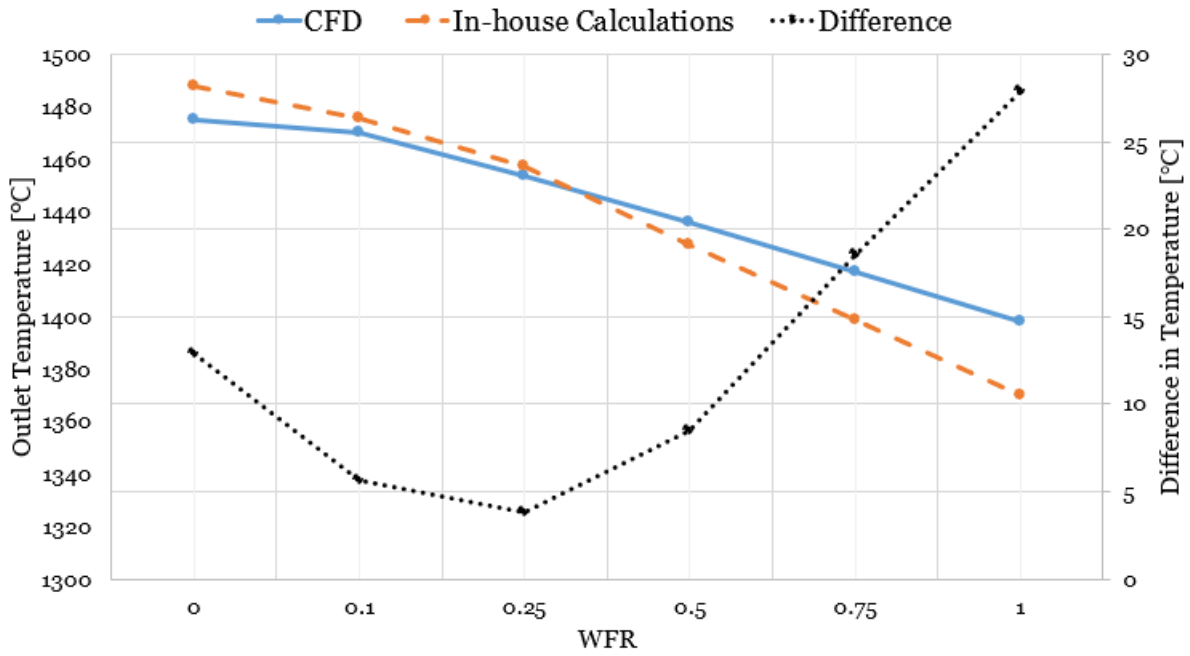

Figure 22 : Comparison of CFD and In-house calculations for non-premixed Diesel + air case. SCM outlet temperature is on the left axis but on the right axis, the difference between CFD and In-house calculations as a function of WFR.

5. Discussion

In the discussion section of this thesis, the focal point is the significant discoveries of the research and their implications. Therefore, the primary aim of this section is to provide a detailed analysis of the results that can contribute to the existing knowledge in the field and offer new insights into the research questions and objectives of this thesis.

5.1 Methodology for SCM in STAR CCM+

Adding water to a gas turbine's combustion process has recently garnered significant attention. However, as far as current research indicates, studies have yet to be conducted in this field of gas turbine combustion comparable with this thesis's scope or methodology. Furthermore, although studies have explored the effects of injecting water into the combustion process, they have used mainly different CFD tools (software) and were not explicitly focused on gas turbine combustion. Given the limited research in this area, the methodology for this thesis project has been developed based on the available information in the STAR CCM+ user guide, as well as the in-house experience of the SE combustion team.

The SGT-800 gas turbine combustor geometry has been simplified for fast turnaround and good convergence. As a result, the computational cost has been reduced due to the small computational domain, and it was easy to identify problems. Furthermore, the polyhedral cell was used for meshing, which is suitable for multi-directional flow and computationally efficient.

The FGM model was used for modeling combustion. This model is considered the most precise among flamelet models and is computationally cheap according to STAR CCM+ (26). However, the flamelet method has several limitations which could impact the accuracy of the solution. The flamelet method cannot account for the impact of the three-dimensionality of the flow field on the flame structure, the decoupling of chemistry and transport, and the failure to capture the finest chemistry-turbulence interactions (19). Flamelet method greatest advantage lies in its computational efficiency since flamelet models pre-calculate the chemistry in gas-phase laminar flames using simple 0D or 1D geometries with detailed chemical mechanisms and use a reduced set of variables to parameterize and tabulate the species from these simple flames. These pre-computed laminar flames, known as flamelet library tables that do not consider the finest chemistry–turbulence interactions, are then interpolated in the 3D simulation of turbulent flames. The FGM model assumes that the chemical states observed in turbulent flames are similar to those found in laminar flames (26). These limitations impact the accuracy of the flamelet model since the flow inside the combustor is three-dimensional and highly unsteady. That is why the complex chemistry model has been implemented for the premixed methane case. It includes sub-models that consider the turbulence-chemistry interactions during simulation. Unfortunately, due to limited time, the complex chemistry model remains incomplete, and some challenges have been faced during simulations which are thoroughly described in Appendix A.4. Nevertheless, upon observing Table A3 in Appendix A.4, it becomes evident that the FGM model yields accurate solution in predicting the mass fractions of water vapor, carbon dioxide (CO_2), and nitrogen molecules, as they closely align with the analytical solution, within a 99 % of accuracy. On the other hand, the complex chemistry model does not exhibit a strong agreement with the analytical solution, indicating the need for a thorough evaluation of the complex chemistry model.

To simulate liquid injection, the Lagrangian multiphase method was employed to track the movement of diesel and water droplets from the spray injector. This method is particularly

useful in systems where a continuous phase has a smaller volume of discrete particles, droplets, or bubbles (26). The Lagrangian multiphase model has worked well in injecting water and diesel droplets. Additionally, the Realizable k-ε Two-Layer turbulence model was chosen for the simulations to capture rotational and swirling flows, and it provides accurate results for moderate-resolution meshes (26).

The addition of water in STAR CCM+ was defined in two ways: as an inert stream and as a third stream. The inert stream does not undergo chemical reactions, while the third stream participates in chemical reactions. Therefore, the FGM table needs to be regenerated; more on this in the next section. In brief, the simulation outcomes indicate that the methodology employed yields reasonable outcomes but with certain limitations that will be elaborated on in the subsequent sections.

5.2 Characteristic of SCM and Comparison

The SGT-800 gas turbine combustor model was simplified to a 30-degree cut of the entire model, which includes a mixing tube, one pilot, chamber walls, and a pressure outlet. CFD simulations have been performed in STAR CCM+ on the SCM to save computational time and easy to mitigate challenges. The CFD simulation conducted for the SCM demonstrated good alignment with both the theoretical expectations and the findings of D. Moëll et al. in their research (17) regarding gas turbine combustion.

For premixed Methane + Air case velocity magnitude, mass fraction of CH4 and temperature field inside the SCM is presented in Figure 13-Figure 15, respectively. As mentioned in the theory section 2.1, the highest velocity is seen in the center of the mixing tube. Vortex breakdown occurs when swirl flow is expanded into the combustion chamber, which is noticeable in Figure 13 (16). Furthermore, Figure 13 is well aligned with Figure 4 and vortex breakdown, which creates a large vortex structure and a central recirculation, and an outer zone is presented for the SCM.
A high gradient of velocity and temperature exists near the chamber walls of the SCM, which is not included in the mesh refinement region. To accurately capture this gradient, it would be beneficial to expand the refinement region. However, since the difference between the refinement and base regions is not substantial, this expansion may only have a minor effect on the mass flow average temperature at the outlet. Moreover, the mass fraction of CH4 and temperature field match well in Figure 14 and Figure 15. The hottest temperature inside the SCM is presented in the region where mass fraction of CH4 is zero, meaning combustion has occurred, and all fuel is burnt. Chemical energy is transferred to thermal energy. Inside the mixing tube of the SCM, the temperature is low, and a mass fraction of CH4 is presented, meaning that no combustion has occurred, thus no flashback inside the mixing tube.

The steady-state flame shape visualized by the progress variable and vorticity magnitude of the SCM is compared with D. Moëll et al. CFD simulations for the entire SGT-800 combustor for the premixed methane mixture are in Figure 16 and Figure 17 (17). The results in Figure 16 show that the flame shape of the SCM closely agrees with the authors' work, as both predict a similar flame shape close to the mixing tube outlet. The highest vorticity was observed at the center of the SCM mixing tube, which is aligned with the finding of D. Moëll et al. simulations. Additionally, a vortex breakdown is observed at the outlet of the mixing tube in Figure 16 and Figure 17 which also agrees with Figure 4. However, it should be noted that D. Moëll et al. CFD results are from unsteady RANS simulations where the flame shape is presented by time-averaged mean flame front and the vorticity magnitude field is instantaneous. However, the goal is to indicate if SCM captures the same pattern and flame shape as D. Moëll et al. CFD simulations, which agree well with the experimental results according to SE.

Furthermore, in Figure 18flame shape is unstable and more diffuse, and the temperature field is unevenly spread for non-premixed Methane + Air and Diesel + Air compared to premixed

Methane + Air. On the contrary, the flame shape for the premixed methane mixture is conical and has a stable front edge shown in Figure 15. The difference between the flame shape and temperature field between premix mixture and non-premixtures can be because fuel and air are mixed before entering the SCM for the premixed case, creating homogenous mixture. In contrast, for non-premixed cases, a non-uniform (inhomogeneous) mixture of fuel and oxidizer is seen inside the mixing tube as presented in Figure 19.

The flame shape instability shown in Figure 18b, and the outlet temperature fluctuations presented in Figure 20 for diesel cases may have multiple contributing factors. One significant factor is the flow's unsteadiness and complexity of diesel fuel combustion, which is challenging to capture using steady-state simulations. In Appendix A.3, various solver set-ups and schemes were tested in response to the outlet temperature fluctuations observed in the diesel case. It was found that employing a first-order scheme with a low relaxation factor resulted in a converged solution, with the outlet temperature stabilizing. On the other hand, using a second-order scheme proved to be challenging in terms of convergence, and the outlet temperature exhibited fluctuations. First-order with low under-relaxation factors gives a converged solution. However, the accuracy of the first-order scheme remains a concern since the second-order scheme is numerically more accurate than the first-order scheme (21). However, the changes in the solution due to the use of low under-relaxation factors or a first-order scheme create difficulties in placing trust in the results obtained. Consequently, these alterations in settings introduce additional uncertainties associated with the methodology.

Moreover, Diesel fuel simulations are more complex than those using methane fuel due to the inclusion of multiphase modeling and evaporation of diesel fuel particles. Although steady-state RANS can capture the overall characteristics of combustion, their limited temporal resolution makes it challenging to accurately predict unsteady phenomena such as flame stabilization, combustion instabilities, thermoacoustic instabilities, and self-ignition (33). Additionally, combustion systems are dynamic and unsteady and averaging eliminates the dynamic and intrinsic coupling between flow and chemistry in the underlying reactive process (33). Therefore, a time-resolved method such as Unsteady-RANS, LES or DNS is usually required to capture the effects of unsteadiness in computational studies accurately. However, the high computational cost of using reaction mechanisms in LES or DNS limits their applicability for this project. In this project, the focus is on predicting the mass flow average temperature at the combustor outlet. Since the aim is not to capture the unsteadiness of the flow, RANS simulations are considered sufficient on a reasonable basis.

5.3 Water Effects on Parametric Cases

A parametric study has been conducted using gas and liquid fuel for the SCM. Both premixed and non-premixed combustion of methane were modeled, while the diesel fuel mixture was only modeled as non-premixed. The simulation results for the parametric cases presented in section 3.2 were successfully run in STAR CCM+ and comparison is summarized in Table 3. From Table 3, where water is defined as an inert stream, it can be noticed that when water (WFR =0.5) is added to the premixed methane mixture or non-premixed diesel case, the outlet temperature drops by approximately 39 ℃ in both cases. On the other hand, for the non-premixed case, the outlet temperature drops by 43 ℃, which is 3.8 ℃ greater than the premixed methane mixture. Additionally, in the premixed methane case, introducing water as vapor results in a temperature drop of only 19.1 ℃, roughly 50% lower than that observed with pure water injection. This is because the vapor has the same temperature as hot air at the inlet of the combustor. In contrast, the temperature of the water is 15 ℃, which requires more energy to evaporate, leading to a significant reduction in the outlet temperature. On the other hand, for the diesel case, when water is premixed as a mixture of emulsion, the temperature drop is 52.8 ℃ which is 35 % higher than simply adding water.

However, when water addition is defined as a third stream in Table 4 the results vary approximately by 3 ℃ for methane mixtures and Diesel + Water + Air case. For the emulsion case, the difference is 15.6 ℃ between the inert and third streams. When water is defined as a third stream, it will take part in chemical reactions, and thus the FGM table must be regenerated, whereas the inert stream is non-reacting and does not take part in the FGM table. The inert model solves a transport equation for the inert mass fraction, and the 3-stream solves a transport equation for the 3-stream mixture fraction. The difference is that mixture properties (e.g., density, species) are calculated from the flamelet manifold table (e.g., chemical equilibrium) for 3-stream. In contrast, for the inert stream, the mixture properties are calculated as the mass-weighted average of 2-stream and inert properties (26). Whether water is defined as a third stream or inert stream does not significantly impact the final solution since the difference is only 0.25 %, most likely due to the difference in solving the transport equations.

In Appendix A.2 for determining the mixture temperature numerically and analytically, the results indicate a difference of 6.3 ℃ between the analytical and numerical solutions, suggesting that STAR CCM+ underestimated the mixture temperature by approximately 1.56%. Additionally, the impact of water addition on temperature drop was examined using both STAR CCM+ and analytical calculations. It was observed that STAR CCM+ overestimated the outlet temperature by 3.7 ℃, representing an overprediction of 1% when water was introduced. Notably, the analytical solution assumes a constant specific heat coefficient, whereas STAR CCM+ incorporates a temperature-dependent coefficient, resulting in a more realistic representation. For further details on this case, see Appendix A.2.

In Figure 21 and Figure 22 WFR is varied for premixed methane and non-premixed diesel cases, respectively. Outlet temperature from CFD simulations, in-house calculation and Cantera is plotted on the left axis, where the difference is on the right axis. The difference between the in-house calculations and CFD simulation for the premixed methane and non-premixed diesel case is non-linear as the amount of water (WFR) increases. The lowest difference for methane mixture is 4℃ when WFR is 0.5 and the highest of 24 ℃ when WFR is 0 (pure methane). On the other hand, for non-premixed diesel cases, CFD simulation underpredicts the in-house calculation when WFR is less than 0.25 and overpredicts above 0.25. One should remember that the maximum limit for CFD simulations to be good enough is a difference of 10 ℃ with in-house calculations. For vapor case and methane-air cases with water addition Cantera results agrees well with CFD simulations for WFR between 0 to 0.5.

Upon close examination of Figure 21 and Figure 22, it is evident that the methane and diesel mixtures, with the addition of water, consistently surpass the 10 ℃ limit for a significant part (values) of the plot. Several factors can contribute to this outcome, including limitations within the in-house calculations, shortcomings in the reaction mechanism, and the constraints of FGM combustion modeling discussed earlier. It is essential to acknowledge that the in-house calculation sheet has its own limitations and discrepancies compared to CFD simulations. These differences involve aspects such as applying thermodynamic and kinetic data for various chemical species, reaction mechanisms, rounding errors in specific heat coefficients, and variations in fuel temperature and air composition. Due to these limitations, the in-house calculation sheet tends to overpredict the outlet temperature by approximately 0.2-0.5%, which, in this case, can result in a deviation of approximately 2.9-7.25 ℃ (assuming a baseline value of 1450 ℃). The difference of 2.9-7.25 ℃ from the actual value poses challenges in achieving the 10 ℃ limit, especially considering the additional limitations of CFD simulations that contribute to this difference. According to SE, Cantera is considered to be more accurate than the in-house calculations, which explains the smaller differences observed between Cantera and CFD simulations for WFR between 0 to 0.5 and for vapor case. However, even with Cantera, the temperature difference increases to 27.9 ℃ for a WFR of 1.

Furthermore, it should be noted that the composition and thermodynamic properties of the diesel fuel differ between the in-house calculation sheet and STAR CCM+, introducing another source of error. As discussed earlier, the diesel case is particularly complex, and the solution changes when altering the scheme or reducing the under-relaxation factors. Consequently, it is challenging to draw any definitive conclusions regarding the accuracy of the diesel simulations. For further discussion on diesel fuel simulations, see Appendix A.3. Moreover, drawing conclusions for the emulsion and vapor cases is also challenging since the in-house calculation sheet cannot calculate the outlet temperature for these scenarios. Nevertheless, both cases obtain realistic CFD results.

Moreover, uncertainties in CFD simulation can be due to the use of reaction mechanisms. The combustion of methane and diesel fuel has been modeled using the GRI 3.0 and Z65 kinetic mechanisms, respectively. However, there are many other reaction mechanisms available for this purpose. Compared to diesel fuel, chemical kinetics mechanisms for methane/air combustion are well-established and can predict combustion characteristics across a range of conditions. Nevertheless, uncertainties persist in extreme conditions like low temperatures and high pressures in real-world combustion applications (33)- (34). One limitation of these mechanisms is that they are primarily developed for burning pure fuels in dry air, whereas real systems may have higher levels of water vapor and exhaust gas recirculation, leading to increased CO_2 levels (35). Additionally, real systems are never completely dry, and the presence of H_2O will vary depending on temperature and other conditions (35). Although there are few mechanisms validated for fuel mixed with water, there is a need for simplified kinetic schemes for use in computational fluid dynamics simulations. Fisher and Jiang's analysis of ignition delay simulation results shows that the chemical kinetics of methane combustion combined with H_2, CO, or CO_2 is not yet fully understood, and even highly detailed mechanisms cannot accurately represent the chemistry (36). Despite the incomplete understanding of combustion chemistry, simplified kinetic schemes are needed for use in CFD simulations. It may be necessary to conduct sensitivity studies on kinetic mechanisms, and the current mechanism may not be suitable for water injection and multi-component fuel (vapor and emulsion). Therefore, testing of new kinetic mechanisms for both fuels is desired. Reaction mechanisms in theory could include all possible species and reactions, but in reality, they are limited by computational time and knowledge of which species and reactions to include. Thus, each mechanism has a range of conditions where it has high accuracy in predicting flame parameters (33).

6. Conclusions

In conclusion, the present study successfully used the SCM in STAR CCM+ to model water addition in gas and liquid fuel combustion. The CFD simulations achieved convergence for all parametric cases through the implemented methodology, with the SCM outlet temperature being determined in a reasonable range for each case. The CFD simulation of the SCM showed good agreement with the theory in the field of gas turbine combustion and D. Moëll et al. research (17). The SCM's flame shape and vorticity field closely agree with the D. Moëll et al. research (17). As stated in (1), vortex breakdown happens when swirl flow is expanded into the combustion chamber. STAR CCM+ was able to capture this physical phenomenon through the use of SCM.

Adding water of WFR 0.5 has the same impact on the outlet temperature of SCM for both premixed methane and non-premixed diesel fuel cases. Notably, the outlet temperature drop due to water addition was found to be 3.8 °C greater for the non-premixed methane case compared to the premixed methane mixture. However, when considering vapor, the temperature drop was approximately 50% lower than that observed with pure water injection. In the case of emulsion, the outlet temperature drop was 35% higher than when water was simply added to the diesel fuel. In addition, noteworthy discrepancies between CFD and in-house calculations were observed, with the greatest differences being 24 °C for premixed methane (at WFR of 0) and 28 °C for non-premixed diesel (at WFR of 1). However, the Cantera calculation outcomes for both the vapor and methane cases with water were within a range of 10 °C when compared to the CFD simulation for the WFR values ranging from 0 to 0.5, in contrast to the performed in-house calculations sheet.

The employed FGM combustion model, Lagrangian multiphase model, and RANS simulations yielded promising results with numerous limitations. In addition, the convergence of gas fuel cases was smoother compared to liquid fuel cases, which involved multiphase modelling and evaporation, makes it more complex. Nevertheless, achieving a simulation accuracy within a 10 °C limit proved challenging due to limitations and potential sources of error in the in-house calculation sheet, combustion modelling, RANS simulations, and reaction mechanism.

7. Future Work

SGT-800 combustor has been simplified, and CFD simulations have been performed in STAR CCM+ for liquid and gas fuel with water addition. The employed methodology has obtained realistic results. However, 10 °C limit proved challenging due to limitations and potential sources of error in the in-house calculation sheet, combustion modeling, RANS simulations, and reaction mechanism. Due to the limited time of the project, there were some improvement areas that were not explored or tested. These areas include:

- The FGM combustion model does not consider the finest chemistry–turbulence interactions and the transport equation are solved for few species. This may influence the outlet temperature, which is why the complex chemistry model has been implemented, taking into account these limitations. However, the complex chemistry model resulted in an unrealistic temperature and velocity field. The results are presented in Appendix A.4 for the complex chemistry model and need to be investigated further. In addition, the complex chemistry model remains incomplete due to the limited time in this project.
- Section 5.3 discusses how uncertainties in CFD simulations can arise from reaction mechanisms. These uncertainties can persist in extreme conditions, such as low temperatures and high pressures in real-world combustion applications. Additionally, some reaction mechanisms may only suit certain conditions, creating further complexity. Therefore, conducting a comprehensive study to determine the optimal reaction mechanism or compare multiple mechanisms is essential to ensure accurate results.
- While steady-state RANS simulations can provide an overall understanding of combustion and obtain reasonable outlet temperature, their limited temporal resolution poses challenges in accurately predicting unsteady flow phenomena. Combustion systems are inherently dynamic and unsteady, and averaging in RANS eliminates the intrinsic coupling between flow and chemistry. Therefore, to capture the effects of unsteadiness in computational studies, it is often necessary to employ time-resolved methods such as URANS (Unsteady RANS), LES, or DNS. However, the high computational cost of incorporating reaction mechanisms in LES or DNS restricts their applicability in this project. In the future, running time-resolved simulations may offer more accurate results and help address the challenges posed by diesel and complex chemistry cases.

8. Perspectives

In this chapter, the societal and commercial implications of the thesis are briefly discussed.

The primary objective of the thesis was to enhance understanding regarding incorporating water into the combustion of gas and liquid fuels within the simplified gas turbine combustion chamber. Therefore, this research is focused on evaluating the available methodologies in Star CCM+ for modelling water injection in SCM using liquid (diesel) and gas (methane) fuels. Additionally, the thesis validated the capability of STAR CCM+ for predicting flame temperature at the outlet against in-house calculation data for the parametric cases. As a result, this research is expected to enhance the understanding of the methodology for adding water into the combustion process using CFD software STAR CCM+.

The thesis's findings are unlikely to have a significant impact on gender and socio-economic perspectives.

References

1. **El-Sayed, Ahmed F.** *Aircraft propulsion and gas turbine engines*. Boca Raton : Taylor & Francis Group, 2017. 9781466595163.
2. **GE Energy.** *Addressing Gas Turbine Fuel Flexibility*. s.l. : GE Energy, 2011. GER4601.
3. **Agbadede, Roupa and Allison, Isaiah.** *Effect of Water Injection into Aero-derivative Gas Turbine Combustors on NOx Reduction*. Nigeria : European Journal of Engineering Research and Science, 2020. 2020.5.11.2180 .
4. **Sharafoddini, R., Habibi, M. and Pirmohammadi, M.** *Numerical Study of Water Vapor Injection in the Combustion Chamber to Reduce Gas Turbine Fuel Consumption* . Tehran : Islamic Azad University, 2019. 1735-3572.
5. **Bulat, G., Marquis, A.J. and Jones, W.P.** *Large Eddy Simulation of an industrial gas-turbine combustion chamber using the sub-grid PDF method*. London : Imperial College London, 2012. 3155-3164.
6. **Inam, Syed Azeem, Hussain, Mukkarum and Baig, Mirza Mehmood.** *Numerical Simulation of Liquid Fuel Injection in Combustion Chamber*. Islamabad : King Fahd University of Petroleum & Minerals, 2019. 44:5889–5895.
7. **Chen, Xiaoyu, et al.** *Numerical Analysis of the Combustion in Micro Gas Turbine with Methane/Biogas Fuels*. Shanghai : King Fahd University of Petroleum & Minerals, 2021. 46:11897–11907.
8. **Nguen, T. D., et al.** *Experimental and Numerical Investigation of the Mixing Ratio for Various Vane Swirlers of the Combustion Chamber of a Gas Turbine Engine*. Tatarstan : Allerton Press, Inc., 2019. 1068-7998.
9. **Gil, Mario Belmar.** *Computational study on the non-reacting flow in Lean Direct Injection gas turbine combustors through Eulerian-Lagrangian Large-Eddy Simulations*. Valencia : Universitat Politècnica de València, 2021.
10. **Persson, Marcus.** *Combustion modelling using spray injectors in gas turbines*. Linköping : Linköping university, 2018.
11. **Kuznetsov, V A, et al.** *Numerical study of the effect of superheated steam supply during the combustion of liquid fuel in a burner on the reduction of harmful emissions*. Krasnoyarsk : IOP Publishing Ltd, 2021. 2233.
12. **Lörstad, Daniel, et al.** *MEASUREMENTS AND LES OF A SGT-800 BURNER IN A COMBUSTION RIG* . s.l. : ASME, 2012. 978-0-7918-4468-7.
13. **Mannerfolt, Anton and Magnusson, Rikard.** SGT-800 - Combustion Support. *SIEMENS-ENERGY*. [Online] SIEMENS-ENERGY, 04 09, 2022. [Cited: 02 16, 2023.] https://wiki.siemens-energy.com/display/more/SGT-800+-+Combustion+Support.
14. **Lörstad, Daniel, et al.** *SIEMENS SGT-800 INDUSTRIAL GAS TURBINE ENHANCED TO 50MW: COMBUSTOR DESIGN MODIFICATIONS, VALIDATION AND OPERATION EXPERIENCE*. Finspång : ASME, 2013. SE-612 83.
15. **Lönning, Jonathan.** *Experimental Investigation of Fuel Mixing Concepts for 3rd Generation DLE Burners*. Linköping : Linköping University, 2016. 02511.
16. **Syred, Nicholas.** *A review of oscillation mechanisms and the role of the precessing vortex core (PVC) in swirl combustion systems*. Cardiff : Elsevier, 2006. 0360-1285.

17. **Moëll, Daniel, Lörstad, Daniel and Bai, Xue-Song.** *NUMERICAL INVESTIGATION OF HYDROGEN ENRICHED NATURAL GAS IN THE SGT-800 BURNER*. Finspång : ASME, 2015.
18. **Jonathan H, Frank and Robert S, Barlow.** *Non-premixed Turbulent Combustion*. Livermore : Sandia National Laboratories, 2007.
19. **Palies, Paul.** *Stabilization and Dynamic of Premixed Swirling Flames*. Huntsville : Elsevier Inc, 2020. pp. 273-315.
20. **Rogers, G. F. C. and Mayhew, Y. R.** *GAS TURBINE THEORY*. India : Dorling Kindersley, 2013. 978-81-7758-902-3 .
21. **Versteeg, H. K. and Malalasekera, W.** *An Introduction to Computational Fluid Dynamics*. London : Pearson Education Limited, 2007. 978-0-13-127498-3.
22. **White, Frank M.** *Fluid Mechanics*. New York : McGraw-Hill Education, 2016. 978-0-07-339827-3.
23. **Woelke, Michal.** *Eddy Viscosity Turbulence Models employed by Computational Fluid Dynamic* . s.l. : General Electric Company Polska , 2007.
24. **Bredberg, Jonas.** *On Two-equation Eddy-Viscosity Models*. Gothenburg : CHALMERS UNIVERSITY OF TECHNOLOGY, 2001.
25. **Shih, T.-H., et al.** *A new k-ε eddy viscosity model for high reynolds number turbulent flows*. Cleveland : Elsevier Science Ltd, 1995. 227-238.
26. **SIEMENS.** *Simcenter STAR-CCM+ User Guide*. 2021.
27. **Helldorff, Helge von and Micklow, Gerald J.** *Primary and Secondary Spray Breakup Modelling for Internal Combustion Engine Applications*. Melbourne : Florida Institute of Technology, 2019. 2458-9403.
28. **Bai, Chuanxin, et al.** *Study on Spray Characteristics and Breakup Mechanism of an SCR Injector*. Basel : MDPI, 2022. 12189387.
29. **Cantera.** CANTERA User's Guide. *cerfacs.fr*. [Online] 2017. [Cited: 06 01, 2023.] https://www.cerfacs.fr/cantera/description.php.
30. **Wang, Wei, Cao, Yong and Okaze, Tsubasa.** *Comparison of hexahedral, tetrahedral and polyhedral cells for reproducing the wind field around an isolated building by LES*. Shanghai : Elsevier Ltd, 2021. 0360-1323.
31. **Sosnowski, Marcin, et al.** *Polyhedral meshing in numerical analysis of conjugate heat* . Czestochowa : EDP Sciences, 2018. 02096.
32. **Gregory P. Smith, David M. Golden, Michael Frenklach, Nigel W. Moriarty, Boris Eiteneer, Mikhail Goldenberg, C. Thomas Bowman, Ronald K. Hanson, Soonho Song, William C. Gardiner, Jr., Vitali V. Lissianski, and Zhiwei Qin.** [Online] Berkeley. [Cited: April 3, 2023.] http://combustion.berkeley.edu/gri-mech/version30/text30.html.
33. **Zettervall, Niklas.** *Methodology for developing reduced reaction mechanisms, and their use in combustion simulations*. Lund : Lund University, 2021. 1102-8718 .
34. **Marashi, Seyedeh Sepideh.** *Network Modeling Application to Laminar Flame Speed and NOx Prediction in Industrial Gas Turbines*. Linköping : Linköping University, 2013. 01782.
35. **Nilsson, Elna.** Methane Combustion's Chemical Kinetic Mechanisms. *Encyclopedia*. [Online] Jun 03, 2021. [Cited: 05 07, 2023.] https://encyclopedia.pub/entry/10470 .
36. **Fischer, M. and Jiang, X.** *A chemical kinetic modelling study of the combustion of CH4–CO–H2–CO2 fuel mixtures*. Lancaster : Elsevier, 2016. 0010-2180.
37. **Methane Gas - Specific Heat vs. Temperature.** *The Engineering ToolBox*. [Online] 2005. [Cited: 05 06, 2023.] https://www.engineeringtoolbox.com/methane-d_980.html .

38. Tillmark, Catharina. *Kinetic study of combustion behavior in a gas turbine Influence from varying natural gas composition.* Lund : Lund University, 2006. 0282-1990.

Appendix A

A.1 Challenges with the SCM Geometry

The simplified combustor model presented in Figure A1 did not give realistic simulation results and could not converge. The only difference between this and the current model, which produces realistic results, is the existence of a swirl cone inlet shape. The pilot air inlet is for the combustion air, and the main burner fuel inlet is for the main fuel supply for non-premix cases. Both inlets are upstream of the mixing tub, shown by blue arrows in Figure A. The third inlet is for the pilot fuel supply, situated in the burner tip close to the combustion chamber, shown by the blue circle in Figure A1. The author believes this model's main issue was implementing a reasonable velocity profile (swirl flow direction). The inlet shape needed to be better suited for velocity profiles taken from the original SE combustor model for the GTC-800 combustor. Furthermore, the flow direction normal to the surface of the inlet was also tested but did not give realistic results.

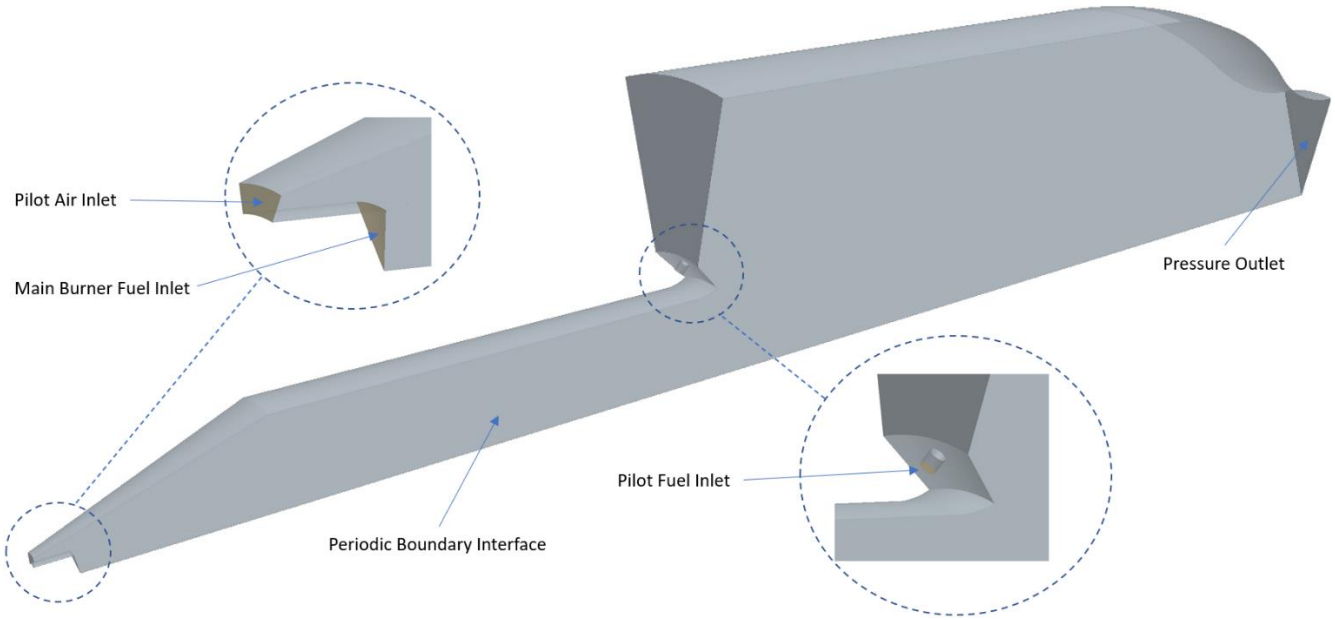

Figure A1: 30-degree cut of simplified combustor model with three inlets and one pressure outlet.

A.2 Comparison of Analytical and Numerical results

This study examines whether CFD simulations conducted in STAR CCM+ yield the same results as analytical calculations regarding the mixture temperature of methane and air and the outlet temperature drop caused by water addition to the SCM. To accomplish this, the analytical calculation of the mixture temperature of methane and air will be compared with the results obtained from CFD simulations at atmospheric pressure.

Accurate inlet temperature for the methane-air mixture is crucial in premixed methane-air cases. The mixture temperature of methane and air can be determined analytically by performing basic thermodynamic calculations based on the conservation of energy. Alternatively, it can be calculated numerically by inputting methane and air as a non-premixed case in STAR CCM+. The thermodynamic properties of air and methane at atmospheric pressure can be found in Table A1.

Table A1: Thermodynamic properties and mass flow rate of methane and air at atm conditions (37).

Material	Initial Temperature [°C]	Cp [j/kg*K]	Mass flow rate [kg/s]
Methane	15	2226	0.000378292
Air	427	1075	0.01438245

Utilizing the first law of thermodynamics and referring to Table A1, the calculated mixture temperature is 405.7 °C. However, applying the same boundary conditions to non-premixed methane-air in STAR CCM+ without combustion yields a mixture temperature of 399.4 °C. This leads to a difference of 6.3 °C between the analytical and numerical solutions, indicating that STAR CCM+ underpredicts the mixture temperature by 1.56 %. Figure A2 displays the mass flow average temperature at the combustor exit during the simulation.

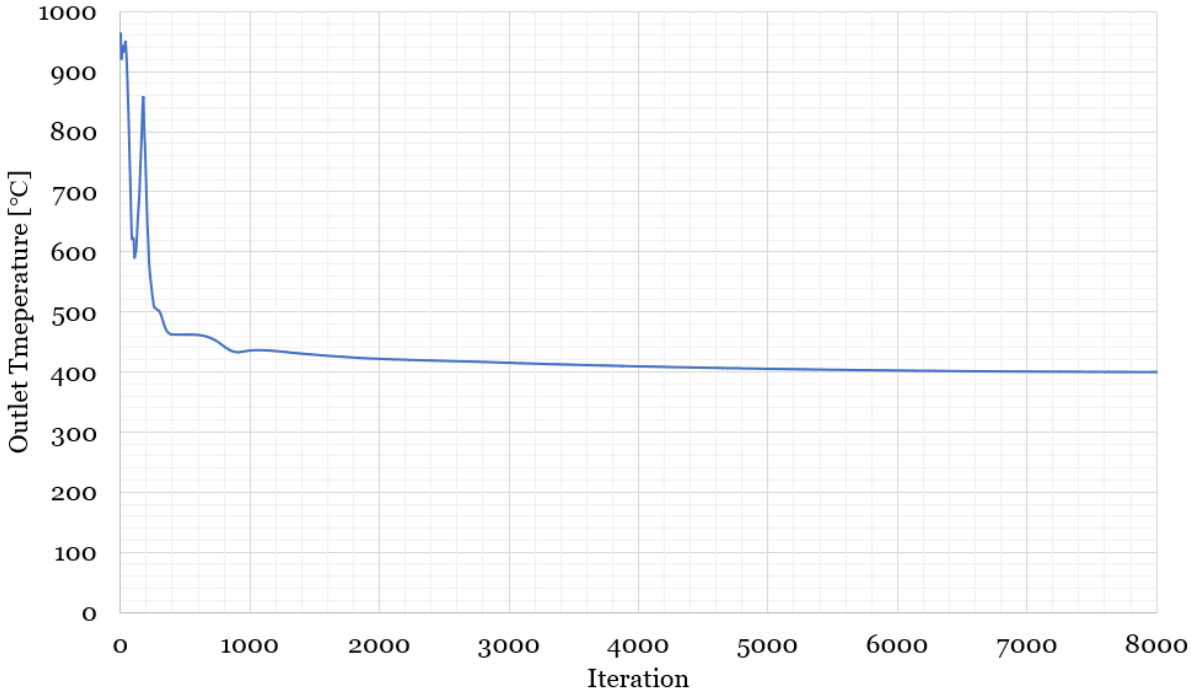

Figure A2: Mass flow average temperature at outlet of SCM for non-premixed methane-air.

In addition, an analytical and numerical calculation has been performed for the premixed methane-air scenario with water injection to determine how STAR CCM+ considers the vaporization of water. Table A2 provides water, methane, and air's thermodynamic properties and mass flow rates. Using basic thermodynamic equations and considering the vaporization energy of water, it can be gathered that the initial temperature of the methane-air mixture, which is 399.41 °C, drops to 368.3°C upon adding water to the mixture.

Table A2: Thermodynamic properties and mass flow rate of methane, air, and water at atm conditions (37).

Material	Initial Temperature [°C]	Cp [j/kg*K]	Mass flow rate [kg/s]
Methane	399.41	3525	0.000378292
Air	399.41	1068	0.01438245
Water	15	4190	0.0001991

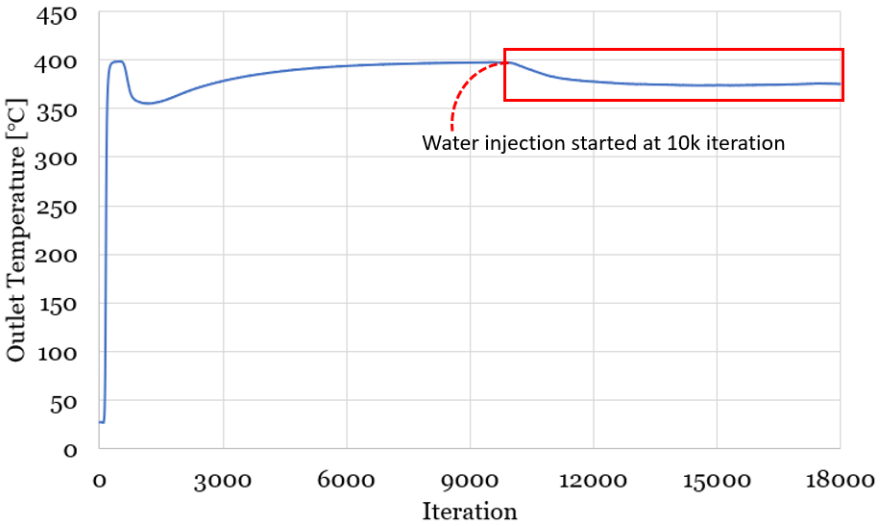

Figure A3: mass flow average temperature at exit of SCM for premixed methane-air with water addition.

The temperature plot at the combustor exit is displayed in Figure A3. The mixture temperature experiences a decline from 399.4°C to 372 °C. A comparison between the analytical calculation and STAR CCM+ shows a difference of 3.7°C, with STAR CCM+ overpredicting the outlet temperature by 1%. Moreover, the temperature drops at the combustor outlet due to water addition is 27.4 °C in STAR CCM+ and 31.1 °C analytically. The particle residence time in Figure A4 illustrates the trajectory of water droplets and indicates that all water transforms into vapor after passing the mixing tube outlet.

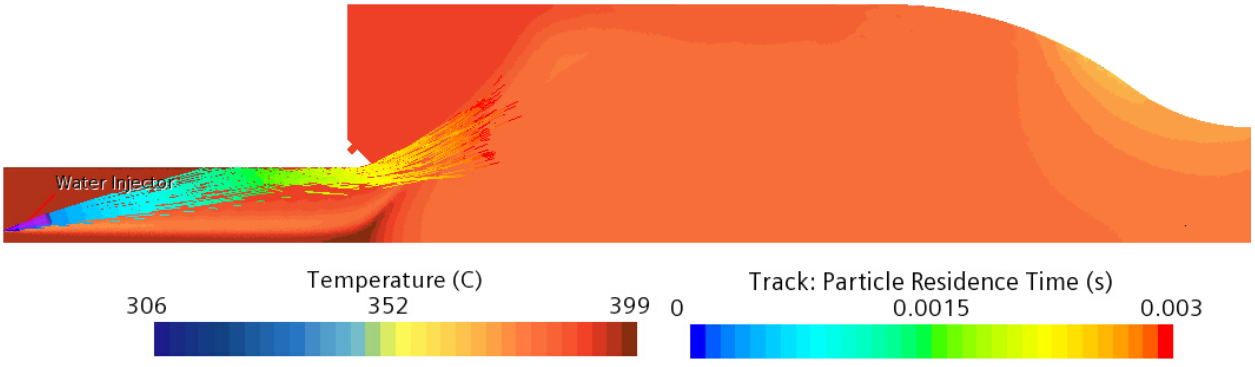

Figure A4: Temperature plot of premixed methane-air inside SCM with water droplet residence time.

A.3 Challenges with Diesel simulations

Unlike methane combustion, the SCM outlet temperature of diesel combustion did not reach a stagnant state. The simulation of diesel fuel combustion involves multiphase modeling and the vaporization process of diesel droplets, making it a challenging problem to solve in a steady-state manner. Various solver configurations were tested to achieve a converged solution and mitigate fluctuations.

As described in the methodology section, all simulations were performed using a second-order scheme, which offers higher accuracy compared to a first-order scheme (21). The default relaxation factor was utilized, as per theoretical considerations indicating that higher under-relaxation factors does not significantly affect the final solution if run for larger number of iterations. Result from certain set-up which was tested for diesel-air case is presented briefly as follow:

1. Second-order scheme with default under-relaxation factors: Mass flow average temperature fluctuates (see Figure A5, and flame shape is unstable (more diffuse), see Figure A4a.
2. First-order Scheme with default under-relaxation factors: Mass flow average temperature is fluctuating but flame shape stable (sharp and conical), see Figure A4b. Residuals also dropped a bit at 115K iterations when switched to first-order scheme, see Figure A6.
3. First-order Scheme with default value of under-relaxation factors reduced by 50%: Mass flow average temperature is not fluctuating, and flame shape is also stable (sharp and conical). Residuals drops a lot at 130K iterations, see Figure A6
4. Second-order scheme with default value of under-relaxation factors reduced by 50%: Mass flow average temperature fluctuates but takes more iterations, see Figure A7, and flame shape is unstable (more diffuse). It is computationally expensive in comparison to other 3 settings.

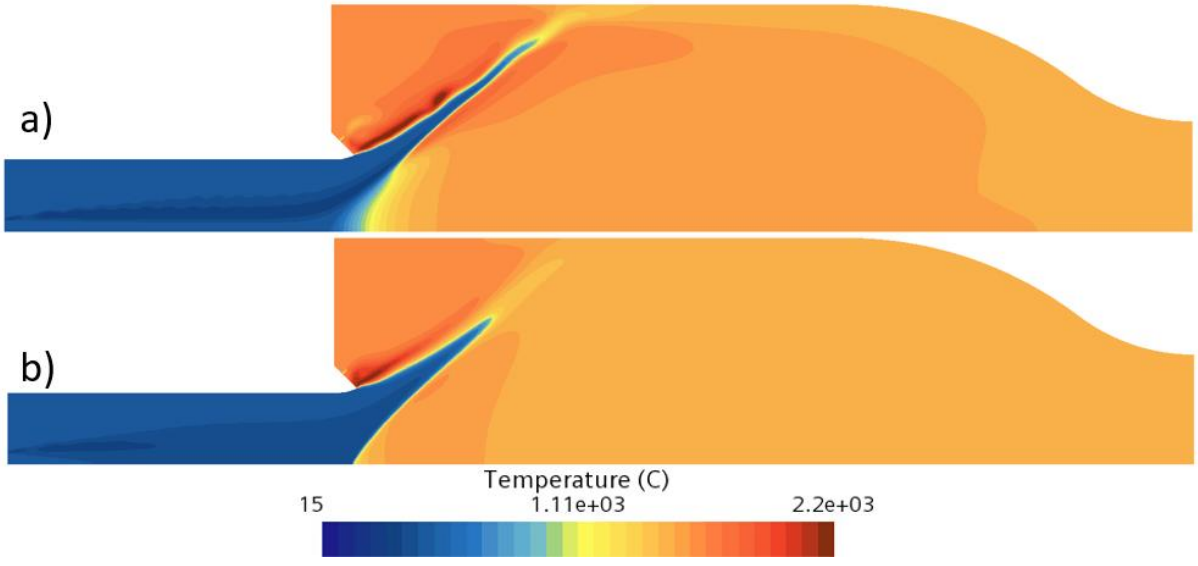

Figure A4: Temperature field inside SCM for Diesel-air case. a) Second-order scheme with default under-relaxation factors. b) First-order Scheme with default under-relaxation factors.

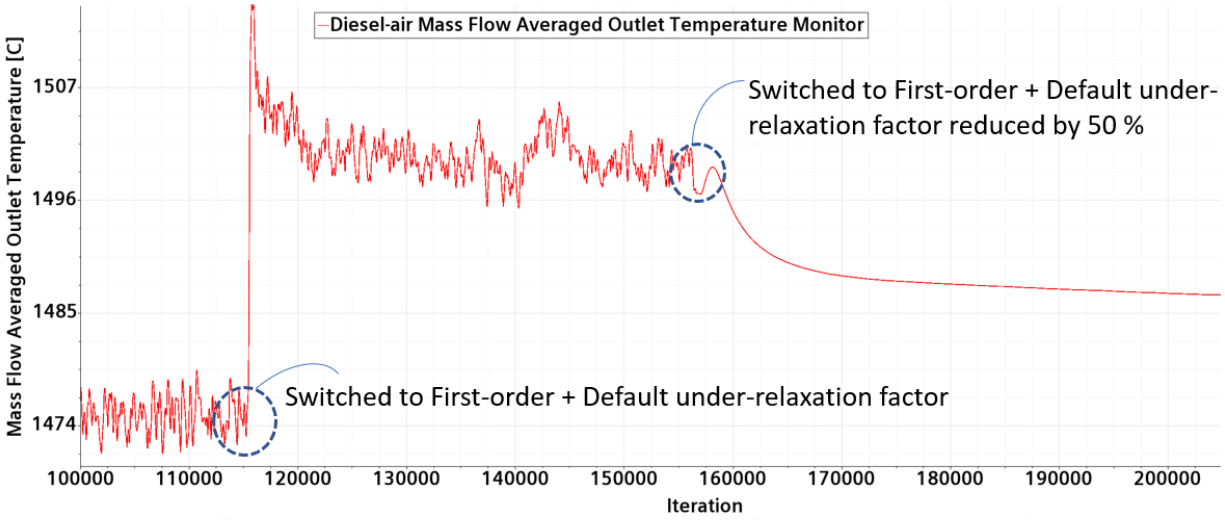

Figure A5: Mass flow average outlet temperature monitor for diesel-air case under certain solver set-up.

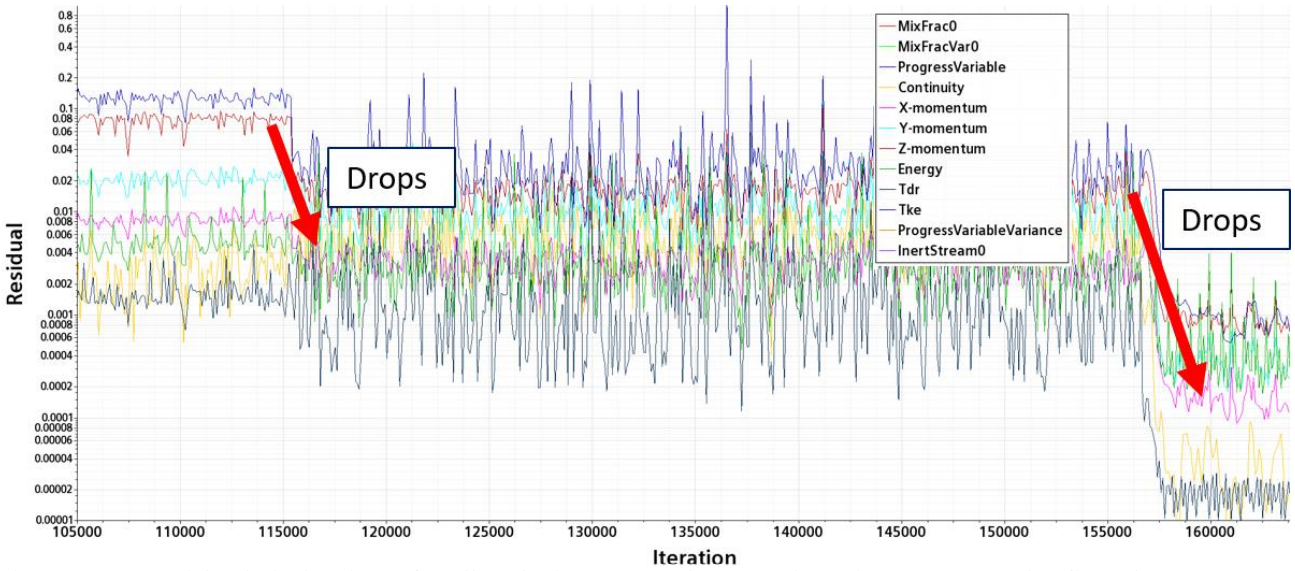

Figure A6: Residuals behaviour for diesel-air case under certain solver set-up. The first drop is due to switching to first-order scheme and the next drop in residual is due to reducing the under-relaxation factor.

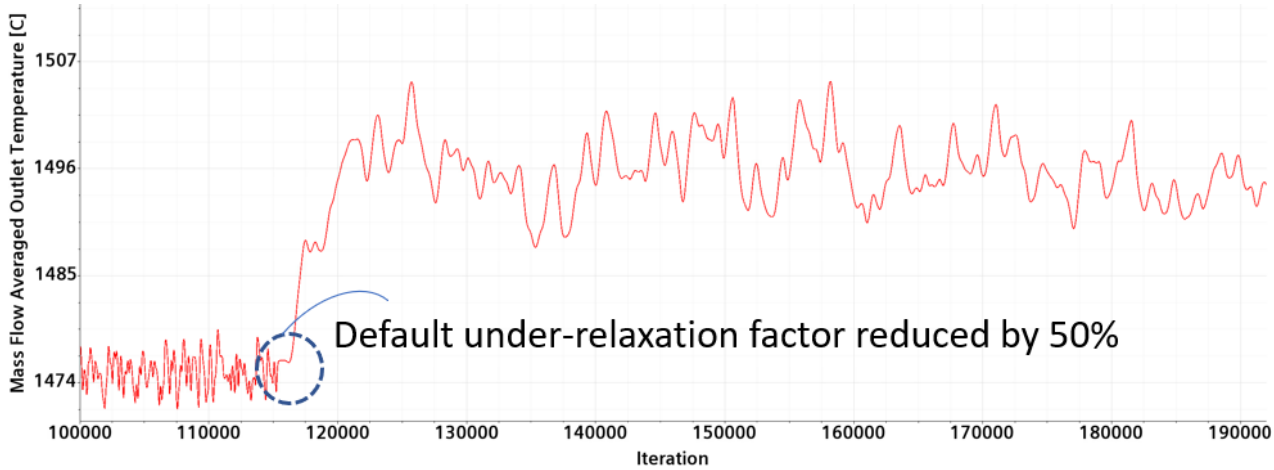

Figure A7: Mass flow average outlet temperature for diesel-air case with default under-relaxation factor reduced by 50%.

In summary, the first-order scheme is a straightforward and computationally efficient method. In addition, it is known for its robustness and stability, mainly when dealing with flows that are discontinuous or highly convective (21). However, its accuracy is limited because it introduces numerical diffusion, which can cause the blurring of sharp gradients of flame shape and loss of fine details in the temperature field in the solution (as shown in Figure A4b). As a result, the first-order scheme may provide less accurate results, especially when trying to resolve complex flow phenomena or capture flow features with high gradients.
On the other hand, the second-order scheme offers higher accuracy by utilizing more advanced numerical techniques. It incorporates central differencing, which considers the values of neighboring cells to calculate spatial derivatives (21). This approach reduces numerical diffusion and preserves the solution's sharp gradients and fine details more effectively (as shown in Figure A4a). However, this increased accuracy comes at the expense of computational complexity and higher computational requirements than the first-order scheme. Although the first-order scheme may produce a converged solution in this case, the accuracy of the simulations remains uncertain. In Figure A8, it is shown that the first-order scheme overpredicts the outlet temperature compared to the in-house calculation for a major part of the plot. In contrast, second-order schemes obtain closer value to the in-house calculations. First-order scheme give closer value for WFR less than 0.1 but as water addition increase (more complexity is added) the difference increases.

The author suggests that the second-order scheme should be utilized despite its higher computational cost when accuracy and capturing fine flow features are essential. Moreover, due to the complex nature of diesel fuel simulations and the highly unsteady nature of the flow field, RANS simulations cannot capture this unsteadiness; time-resolved methods, such as LES or DNS, are usually required (33).

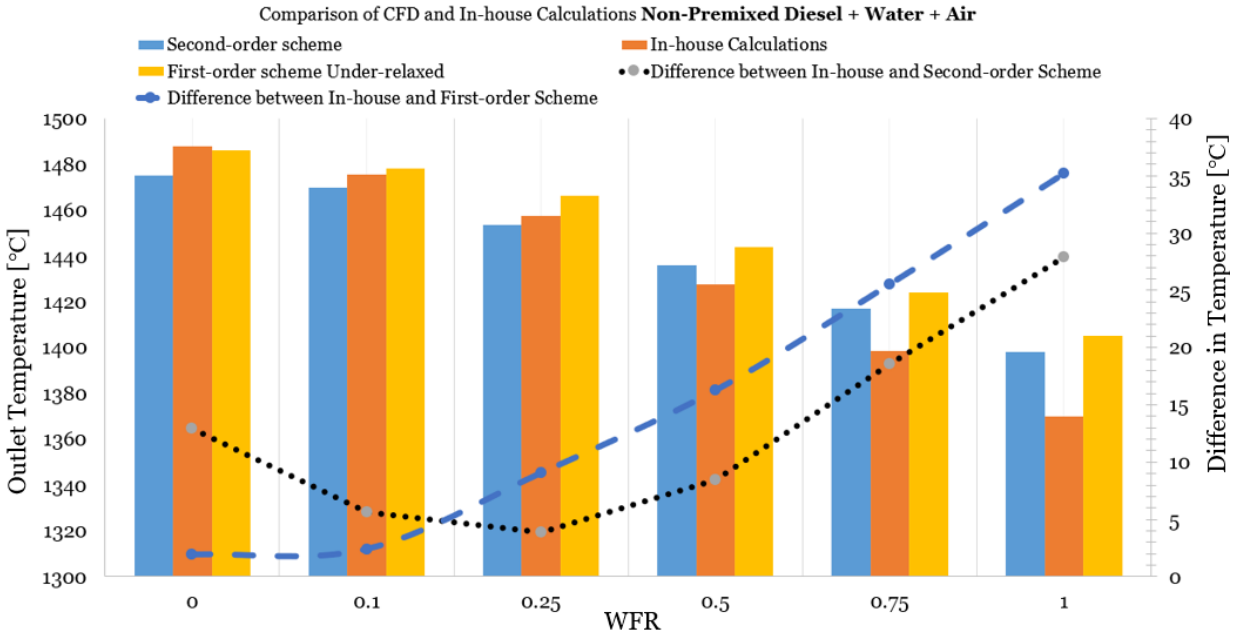

Figure A8: Outlet temperature comparison for second-order scheme and first-order scheme with reduced relaxation-factors for diesel case.

A.4 Challenges with Complex Chemistry Model

The implementation of a complex chemistry model has been applied to premixed methane-air combustion. All other models used for the FGM method are identical, but complex chemistry has been incorporated into the model's tree within STAR CCM+ instead of the FGM method. The same reaction mechanisms utilized for generating the FGM table have been employed to calculate reactions in the complex chemistry models during simulation. In addition, the CVODE solver has been utilized to integrate the chemical source term, and the LFC model has been chosen to account for turbulence effects on combustion. Additionally, clustering has been selected to speed up the simulation of complex chemistry. For more details on implementing complex chemistry, see (26).

However, the initial outcomes from the complex chemistry model appear unrealistic. In the case of premixed methane-air, the outlet temperature deviates significantly from the in-house calculations. Figures A8 and A9 illustrate temperature and velocity fields, revealing unrealistic flow phenomena at the outlet of the mixing tube. The presence of low-temperature and high-velocity regions in the mixing tube is difficult to explain physically. Furthermore, species mass fraction of methane and air combustion, where oxygen (O_2) constitutes 23.3% and nitrogen (N_2) constitutes 76.7%, can be obtained at the outlet through complex chemistry model, FGM model, and analytical calculations. When methane reacts with air, it produces water vapor (H_2O), carbon dioxide (CO_2), and nitrogen molecules, which do not participate in the chemical reaction. For this premixed methane-air case, complete combustion of 0.496 moles of CH_4 requires 0.993 moles of O_2, resulting in an excess of 1.1 moles of O_2. The reaction produces 0.496 moles of CO_2 and 0.993 moles of H_2O. Table A3 presents all the data, comparing the species mass fraction at the combustor outlet obtained from the complex chemistry model, the FGM model, and the analytical calculation. It is worth noting that the analytical solution and FGM model agree within a 2-decimal accuracy.

Moreover, with the second-order scheme and default under-relaxation factor, the outlet temperature does not stabilize for the complex chemistry model and fluctuates between 1700-1630 °C, see Figure A10. Nevertheless, reducing the default under-relaxation factors by 50% results in a stable outlet temperature stagnating toward 1445 °C. The author suggests that RANS simulations may not be the most suitable choice due to the complex chemistry model's high complexity. Instead, time-resolved simulation methods such as LES or DNS should be considered. Unfortunately, due to time constraints in the project, the investigation of the complex chemistry model could not be pursued further and remains incomplete.

Table A3: Mass flow of each species at inlet of combustor and species mass fraction at combustor outlet for complex chemistry, FGM model and analytical solution.

Species Mass fraction at Outlet	Inlet [moles/s]	Complex Chemistry Model	FGM Model	Analytical [Perfect Combustion]
CO_2	0	0.0520	0.07383	0.0739
H_2O	0	0.1301	0.0604	0.0605
N_2	7.8795	0.4488	0.7451	0.7463
O_2	2.0944	0.3161	0.1178	0.1192
CH_4	0.496	0	0.0000	0
Total Mass Fraction		0.9470	0.9971	1.0000000

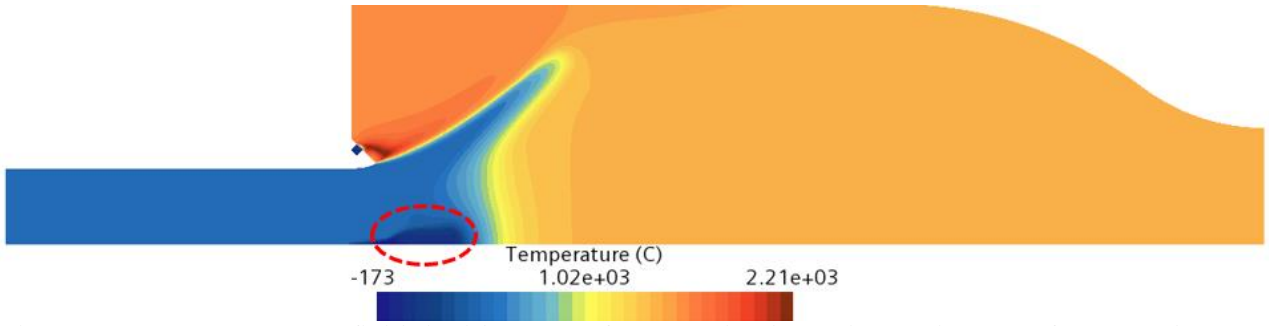

Figure A9: Temperature field inside SCM for premixed Methane-air case for complex chemistry model.

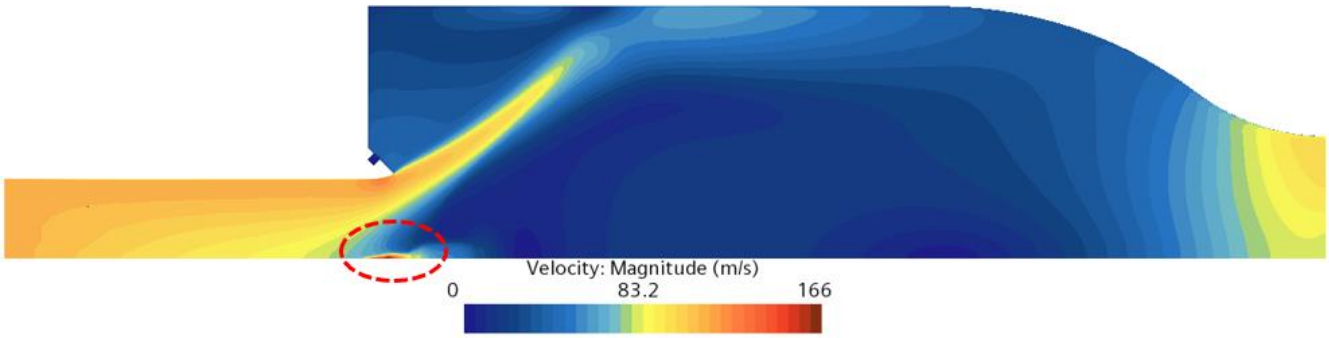

Figure A10: Velocity field inside SCM for premixed Methane-air case for complex chemistry model.

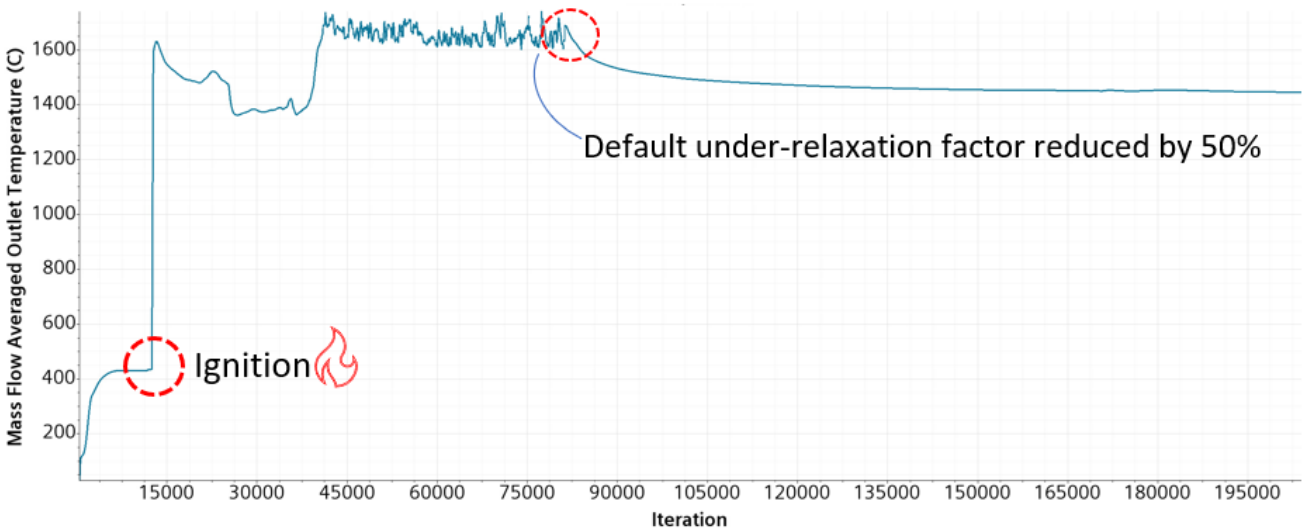

Figure A11: Mass flow average outlet temperature for premixed Methane-air case for complex chemistry model.